

INTRINSIC MIXED FINITE ELEMENT METHODS FOR LINEAR COSSERAT ELASTICITY AND COUPLE STRESS PROBLEM

ANDREA DZIUBEK, KAIBO HU, MICHAEL KAROW, AND MICHAEL NEUNTEUFEL

ABSTRACT. We propose two parameter-robust mixed finite element methods for linear Cosserat elasticity. The Cosserat coupling constant μ_c , connecting the displacement u and rotation vector ω , leads to possible locking phenomena in finite element methods. The formal limit of $\mu_c \rightarrow \infty$ enforces the constraint $\frac{1}{2} \operatorname{curl} u = \omega$ and leads to the fourth order couple stress problem. Viewing the linear Cosserat model as the Hodge-Laplacian problem of a twisted de Rham complex, we derive structure-preserving distributional finite element spaces, where the limit constraint is fulfilled in the discrete setting. Applying the mass conserving mixed stress (MCS) method for the rotations, the resulting scheme is robust in μ_c . Combining it with the tangential-displacement normal-normal-stress (TDNNS) method for the displacement part we obtain additional robustness in the nearly incompressible regime and for anisotropic structures. Using a post-processing scheme for the rotations, we prove optimal convergence rates independent of the Cosserat coupling constant μ_c . Further, we propose a mixed method for the couple stress problem based on the MCS scheme. We demonstrate the performance of the proposed methods in several numerical benchmark examples.

Keywords: Cosserat elasticity; couple stress problem; mixed finite element method; twisted complex; locking

MSC2020: 65N30, 74S05

1. INTRODUCTION

In 1909, the Cosserat brothers [18] introduced the idea to model a material as a collection of points with associated directions that can rotate and stretch independently of the displacement of material points. Günther [26] derived Cosserat equations for linear deformations. A comprehensive review of recent advances including literature on the history of generalized continua and plates and shells can be found in [33]. The Cosserat models have been proven to be effective for various materials with complex microstructure including micropolar fluids and electromagnetic solids (cf. [1]) and man-made Cosserat materials [49]. Identifying the additional material parameters for the microstructure remains challenging (despite Lakes' pioneering size-effect experiments, cf. [32]). However, the number of the material parameters could be reduced through mathematical analysis [36, 35].

There have been extensive studies on the classical elasticity models with finite element methods. An important numerical issue is locking - the convergence may deteriorate or the solution tends to be zero as some physical parameters approach some limit values (an example is when the Poisson ratio ν goes to $1/2$, or equivalently the Lamé constant $\lambda \rightarrow \infty$). Various numerical schemes and finite elements have been proposed to avoid locking. In contrast, numerical schemes for Cosserat models have received less attention, with exceptions such as [48, 50, 45, 25, 58]. Several finite elements have been proposed for two- and three-dimensional linear Cosserat elasticity and the coupled stress problem, which can be obtained as the limit of the Cosserat model for the Cosserat

coupling constant $\mu_c \rightarrow \infty$. To avoid locking problems, a hybrid-stress element has been presented in [58]. For couple stress problems (e.g. for metals, composite polymers, and bone tissues), similar to other high-order gradient theories for elasticity incorporating additional length scales, penalty formulations with selective reduced integration have been used to avoid locking [20, 12, 53, 54, 57]. Cosserat models involve more physical parameters, including a characteristic length scale and three micropolar moduli. Nevertheless, to the best of our knowledge, a method robust with all the parameters for Cosserat and micropolar models and a rigorous numerical analysis are still open. We mention that a recent work [7] constructed a mixed finite element scheme with a rigorous analysis. The method achieves robustness with the limit to classical elasticity (i.e., the coupling constant $\mu_c \rightarrow 0$). However, the limit to couple stress problems ($\mu_c \rightarrow \infty$) was not addressed.

In this paper, we construct schemes for the linear Cosserat problem inspired by Finite Element Exterior Calculus (FEEC) [2, 3, 4]. A key idea of FEEC is to discretize the underlying differential complexes of PDEs. The linear Cosserat model can be viewed as the Hodge-Laplacian problem of the elasticity version of the twisted de Rham complex at index zero [5, 11]. These complexes are intermediate steps for deriving the BGG complexes (e.g., the elasticity complex), and incorporate more information. In the elasticity case, the twisted complex encodes displacement and pointwise rotation, while the elasticity complex (encoding linear elasticity) is obtained by eliminating the variables corresponding to rotation.

Fitting conforming finite elements in the twisted complexes would require higher order smoothness (cf. diagram (2.4)). Instead of pursuing smooth finite elements, we follow the trend of *distributional finite elements*. The idea is to impose weaker regularity and allow Dirac deltas as shape functions. The distributional finite element de Rham complex was initially investigated by Braess and Schöberl [8] for the purpose of equilibrated residual error estimators. Dirac deltas can be paired with fields of proper continuity. This leads to the tangential-displacement-normal-normal-stress (TDNNS) method for linear elasticity [42]. Then the idea has also been applied to Reissner–Mindlin plates [44], the mass conserving mixed stress (MCS) method for Stokes equations [24], and the Hellan–Herrmann–Johnson method for the Kirchhoff–Love plate equation [27, 28, 31] and shells [39, 40]. An attractive feature of distributional elements is that they usually have invariant forms under maps (pullbacks), which is important for finite element computation and generalizations to manifolds. The (affine) invariance reflects certain coordinate independence. For example, in Regge calculus and its finite element interpretation [15, 47], metrics are discretized by the edge lengths, which are coordinate-independent. Therefore these finite elements are intrinsic. We refer to [29, 16] for the construction of distributional finite elements for BGG diagrams and a discrete exterior calculus interpretation.

In this paper we propose two robust mixed finite element methods based on twisted complexes, called the MCS method (Problem 6 below) and the TDNNS-MCS method (Problem 8 below), respectively. Using the MCS discretization method for the linearized rotations with respective couple stress tensor circumvents locking with respect to the Cosserat coupling constant μ_c . When using the TDNNS method for the elasticity part on top of the MCS method, additional robustness for anisotropic structures and nearly incompressible materials is obtained. For the fourth-order couple stress limit problem, for $\mu_c \rightarrow \infty$, a mixed finite element method based on the MCS method is presented avoiding the necessity of H^2 -conforming finite elements which would require a high polynomial degree, stronger and less intrinsic degrees of freedom, and are not available for curved meshes. A rigorous error analysis is performed to prove convergence rates independent of the Cosserat coupling constant μ_c for the proposed mixed formulations. A post-processing procedure for the rotation field is presented. The efficiency and robustness of the proposed methods is demonstrated in several numerical benchmark examples.

The rest of the paper will be organized as follows. In Section 2, we present the equations of linear Cosserat elasticity and the couple stress model and their relation with twisted complexes. In Section 3, we show the two finite element methods. In Section 4 we perform a rigorous error analysis of the proposed methods with respect to the Cosserat coupling constant μ_c . Further, post-processing schemes for the rotation field are discussed. We present several numerical benchmark examples in Section 5 to show the performance and robustness of our methods.

2. LINEAR COSSERAT ELASTICITY AND COUPLE STRESS LIMIT

Let $\Omega \subset \mathbb{R}^3$ be a domain. Define the following algebraic and differential operators for (differentiable) vectors u and matrices A

$$\begin{aligned} \nabla u &= \begin{pmatrix} \frac{\partial u_x}{\partial x} & \frac{\partial u_x}{\partial y} & \frac{\partial u_x}{\partial z} \\ \frac{\partial u_y}{\partial x} & \frac{\partial u_y}{\partial y} & \frac{\partial u_y}{\partial z} \\ \frac{\partial u_z}{\partial x} & \frac{\partial u_z}{\partial y} & \frac{\partial u_z}{\partial z} \end{pmatrix}, & \operatorname{div} u &= \nabla \cdot u, & \operatorname{curl} u &= \nabla \times u, \\ \operatorname{mskw} u &= \begin{pmatrix} 0 & -u_z & u_y \\ u_z & 0 & -u_x \\ -u_y & u_x & 0 \end{pmatrix}, & \operatorname{vskw} A &= \frac{1}{2} \begin{pmatrix} A_{zy} - A_{yz} \\ A_{xz} - A_{zx} \\ A_{yx} - A_{xy} \end{pmatrix}, \end{aligned}$$

and denote by tr , dev , sym , and skw the trace, deviatoric, symmetric, and skew part of a matrix, respectively. The identity matrix is denoted by I . We consider the following material laws

$$(2.1a) \quad C_1(\varepsilon) = 2\mu \operatorname{sym} \varepsilon + \lambda \operatorname{tr} \varepsilon I + \mu_c \operatorname{skw} \varepsilon = \mathcal{C}(\varepsilon) + \mu_c \operatorname{skw} \varepsilon, \quad \mathcal{C}(\varepsilon) = 2\mu \operatorname{sym} \varepsilon + \lambda \operatorname{tr} \varepsilon I,$$

$$(2.1b) \quad \begin{aligned} C_2(\varepsilon) &= (\gamma + \beta) \operatorname{sym} \varepsilon + \alpha \operatorname{tr} \varepsilon I + (\gamma - \beta) \operatorname{skw} \varepsilon \\ &= (\gamma + \beta) \operatorname{dev} \operatorname{sym} \varepsilon + \frac{3\alpha + \beta + \gamma}{3} \operatorname{tr} \varepsilon I + (\gamma - \beta) \operatorname{skw} \varepsilon, \end{aligned}$$

where \mathcal{C} is the classical elasticity tensor with *Lamé parameters* $\mu > 0$ and $\lambda \geq 0$, $\mu_c \geq 0$ is the *Cosserat coupling* constant, and $\alpha, \beta, \gamma \in \mathbb{R}$ are additional so-called *micropolar moduli*.

In the linear Cosserat setting we consider the displacement field $u : \Omega \rightarrow \mathbb{R}^3$ and the rotation matrix identified with its axial rotation vector $\omega : \Omega \rightarrow \mathbb{R}^3$. The *Cosserat energy functional* (with external body forces f_u and f_ω) is defined by, see e.g. [35],

$$(2.2) \quad \begin{aligned} \mathcal{E}^{\operatorname{Cosserat}}(u, \omega) &:= \int_{\Omega} \left(\frac{1}{2} \|\nabla u - \operatorname{mskw} \omega\|_{C_1}^2 + \frac{1}{2} \|\nabla \omega\|_{C_2}^2 - \langle f_u, u \rangle - \langle f_\omega, \omega \rangle \right) dx \\ &= \int_{\Omega} \left(\frac{1}{2} \|\operatorname{sym} \nabla u\|_{\mathcal{C}}^2 + \mu_c \|1/2 \operatorname{curl} u - \omega\|^2 + \frac{\gamma + \beta}{2} \|\operatorname{sym} \nabla \omega\|^2 \right. \\ &\quad \left. + \frac{\gamma - \beta}{4} \|\operatorname{curl} \omega\|^2 + \frac{\alpha}{2} \|\operatorname{div} \omega\|^2 \right) dx - \int_{\Omega} (\langle f_u, u \rangle + \langle f_\omega, \omega \rangle) dx. \end{aligned}$$

The, in general non-symmetric, strain field $\varepsilon = \nabla u - \operatorname{mskw} \omega$ is called the *first Cosserat stretch* tensor and $\kappa = \nabla \omega$ the *micropolar curvature* tensor. Note that (2.2) yields a minimization problem.

Remark 1. For material law C_2 (2.1b) there are several conditions on α , β , and γ to obtain a well-defined energy. It is possible to obtain a positive definite tensor by requiring $\alpha, \beta, \gamma > 0$, however, one can relax the conditions to positive semidefinite, as long as a Korn type inequality holds [30]. General conditions to guarantee non-negativity are, cf. the arising constants in (2.1b),

$$\gamma + \beta \geq 0, \quad 3\alpha + \beta + \gamma \geq 0, \quad \gamma - \beta \geq 0.$$

Depending on different common choices the curvature energy simplifies to, cf. [35],

- (1) pointwise case $\frac{\gamma}{2} \|\nabla \omega\|^2$, corresponding to $\alpha = \beta = 0$,

- (2) symmetric case $\gamma \|\text{sym } \nabla \omega\|^2$, corresponding to $\alpha = 0$ and $\beta = \gamma$,
- (3) deviatoric case $\frac{\gamma}{2} \|\text{dev } \nabla \omega\|^2$, corresponding to $\beta = 0$ and $\alpha = -\frac{1}{3}\gamma$,
- (4) conformal case $\gamma \|\text{dev sym } \nabla \omega\|^2$, corresponding to $\beta = \gamma$ and $\alpha = -\frac{2}{3}\gamma$.

All four cases are well-defined if $\gamma > 0$ and reduce the number of parameters to one, which is often set to $\gamma = \frac{\mu L_c}{2}$, where $L_c > 0$ is the characteristic length of the microstructure.

Let $\Omega \subset \mathbb{R}^3$ be a bounded Lipschitz domain. We split the boundary $\Gamma = \partial\Omega$ into a Dirichlet Γ_D and Neumann Γ_N part such that $\Gamma_D \cup \Gamma_N = \Gamma$ and $\Gamma_D \cap \Gamma_N = \emptyset$, and we denote the outer unit normal by n . Assume that Dirichlet data u_D and ω_D are prescribed on Γ_D and that surface traction forces are given on Γ_N by g_u and g_ω . For simplicity, we assume throughout the paper that the Dirichlet parts for u and ω coincide, and emphasize that the extension to distinguished boundary parts for the displacement and rotations is straightforward. By taking variations of (2.2) with respect to u and ω and integration by parts we readily obtain the strong form with corresponding boundary conditions of linear Cosserat elasticity. By defining the *elasticity stress tensor* $\sigma := \mathcal{C}(\text{sym } \nabla u)$ and the *couple stress tensor* $m := C_2(\nabla \omega)$ we have

$$\begin{aligned}
 (2.3a) \quad & -\text{div}(C_1(\nabla u - \text{mskw } \omega)) = -\text{div}(\sigma) + \mu_c \text{curl}(1/2 \text{curl } u - \omega) = f_u \quad \text{in } \Omega, \\
 (2.3b) \quad & -\text{div}(m) - 2\mu_c(1/2 \text{curl } u - \omega) = f_\omega \quad \text{in } \Omega, \\
 (2.3c) \quad & u = u_D, \quad \omega = \omega_D \quad \text{on } \Gamma_D, \\
 (2.3d) \quad & \sigma_n + \mu_c(1/2 \text{curl } u - \omega) \times n = g_u, \quad m_n = g_\omega \quad \text{on } \Gamma_N,
 \end{aligned}$$

where f_u and f_ω are possible external body forces acting on u and ω , respectively. Further, we use the notation $\sigma_n := \sigma n$ for the normal component of a tensor. Equation (2.3a) is the balance of linear momentum and (2.3b) is the balance of angular momentum.

2.1. Linear Cosserat elasticity as twisted de Rham complex. The Cosserat energy (2.2) corresponds to the *Hodge-Laplacian* problem of the elasticity version of the *twisted de Rham complex* at index zero [11]. This observation motivates our choices of finite element spaces in this paper. In this section, we explain this claim.

The *Bernstein-Gelfand-Gelfand* (BGG) construction in [5, 11] starts with the following diagram:

$$\begin{array}{ccccccc}
 0 & \longrightarrow & [H^q]^3 & \xrightarrow{\nabla} & [H^{q-1}]^{3 \times 3} & \xrightarrow{\text{curl}} & [H^{q-2}]^{3 \times 3} & \xrightarrow{\text{div}} & [H^{q-3}]^3 & \longrightarrow & 0 \\
 & & \searrow \text{mskw} & & \searrow -S & & \searrow -2 \text{vskw} & & & & \\
 (2.4) \quad 0 & \longrightarrow & [H^{q-1}]^3 & \xrightarrow{\nabla} & [H^{q-2}]^{3 \times 3} & \xrightarrow{\text{curl}} & [H^{q-3}]^{3 \times 3} & \xrightarrow{\text{div}} & [H^{q-4}]^3 & \longrightarrow & 0.
 \end{array}$$

Here $[H^q]^3$ denotes a vector-valued function space, for which each component is in the Sobolev space H^q , and $[H^{q-1}]^{3 \times 3}$ denotes the 3-by-3 matrix version, etc. The operator S is defined by $Su = u^T - \text{tr}(u)I$, where u is a matrix and u^T denotes the transpose of u . Both rows of (2.4) are vector-valued de Rham complexes in 3D, which are connected by algebraic operators. One may derive a *twisted de Rham complex* (or, twisted complex, for short) and a *BGG complex* (the elasticity complex) from (2.4). Each space Y^\bullet in the twisted complex consists of two components, one from the first row and one from the second, and the operators d_V^\bullet have the general form

$$d_V^k := \begin{pmatrix} d^k & -S^k \\ 0 & d^k \end{pmatrix},$$

where S^k is the k -th diagonal operator, and d^k denotes the exterior derivative translating into the differential operators used in (2.4). We denote the twisted complex by

$$(2.5) \quad 0 \longrightarrow Y^0 \xrightarrow{d_V^0} Y^1 \xrightarrow{d_V^1} Y^2 \xrightarrow{d_V^2} Y^3 \longrightarrow 0,$$

where $Y^0 = [H^q]^3 \times [H^{q-1}]^3$, $Y^1 = [H^{q-1}]^{3 \times 3} \times [H^{q-2}]^{3 \times 3}$, $Y^2 = [H^{q-2}]^{3 \times 3} \times [H^{q-3}]^{3 \times 3}$, and $Y^3 = [H^{q-3}]^3 \times [H^{q-4}]^3$, and the operators are

$$d_V^0 := \begin{pmatrix} \nabla & -\text{mskw} \\ 0 & \nabla \end{pmatrix}, \quad d_V^1 := \begin{pmatrix} \text{curl} & \mathcal{S} \\ 0 & \text{curl} \end{pmatrix}, \quad d_V^2 := \begin{pmatrix} \text{div} & -2 \text{vskw} \\ 0 & \text{div} \end{pmatrix}.$$

The sequence (2.5) is a complex since $d_V^k \circ d_V^{k-1} = 0$ for all k due to the anti-commutativity condition $dS = -Sd$, which holds for the operators in (2.4). The name “twisted complex” comes from the observation that the operators in (2.5) have an off-diagonal part $-S$, which twists the two de Rham complexes. The aim of the BGG machinery is to eliminate spaces in (2.4) connected by the connecting maps as much as possible, leading to the following BGG complex consisting of the kernels and cokernels of the connecting maps:

$$(2.6) \quad 0 \longrightarrow [H^q]^3 \xrightarrow{\text{sym } \nabla} [H^{q-1}]_{\text{sym}}^{3 \times 3} \xrightarrow{\text{inc}} [H^{q-3}]_{\text{sym}}^{3 \times 3} \xrightarrow{\text{div}} [H^{q-4}]^3 \longrightarrow 0,$$

where $\text{inc} := \text{curl} \circ \mathcal{S}^{-1} \circ \text{curl}$ is the incompatibility operator ($\text{inc } g$ is the linearized Einstein tensor if g is a metric), and $[H^{q-1}]_{\text{sym}}^{3 \times 3}$ denotes the space of symmetric matrices where each entry is a function in the Sobolev space H^{q-1} . This is the most convenient functional analytic setting for deriving the elasticity (BGG) complex. However, to get well-posed formulations of the Hodge-Laplacian problem, we have many other options in the choices of spaces and boundary conditions. For the Cosserat problem, we will use the following variants of (2.5):

$$(2.7) \quad \begin{array}{ccccccc} 0 & \longrightarrow & [H^1]^3 & \xrightarrow{\nabla} & H(\text{curl}; \mathbb{R}^{3 \times 3}) & \xrightarrow{\text{curl}} & H(\text{div}; \mathbb{R}^{3 \times 3}) & \xrightarrow{\text{div}} & [L^2]^3 & \longrightarrow & 0 \\ & & & \nearrow \text{mskw} & & \nearrow -\mathcal{S} & & \nearrow -2 \text{vskw} & & & \\ 0 & \longrightarrow & [H^1]^3 & \xrightarrow{\nabla} & H(\text{curl}; \mathbb{R}^{3 \times 3}) & \xrightarrow{\text{curl}} & H(\text{div}; \mathbb{R}^{3 \times 3}) & \xrightarrow{\text{div}} & [L^2]^3 & \longrightarrow & 0, \end{array}$$

or the version with homogeneous Dirichlet boundary conditions:

$$(2.8) \quad \begin{array}{ccccccc} 0 & \longrightarrow & [H_0^1]^3 & \xrightarrow{\nabla} & H_0(\text{curl}; \mathbb{R}^{3 \times 3}) & \xrightarrow{\text{curl}} & H_0(\text{div}; \mathbb{R}^{3 \times 3}) & \xrightarrow{\text{div}} & [L_0^2]^3 & \longrightarrow & 0 \\ & & & \nearrow \text{mskw} & & \nearrow -\mathcal{S} & & \nearrow -2 \text{vskw} & & & \\ 0 & \longrightarrow & [H_0^1]^3 & \xrightarrow{\nabla} & H_0(\text{curl}; \mathbb{R}^{3 \times 3}) & \xrightarrow{\text{curl}} & H_0(\text{div}; \mathbb{R}^{3 \times 3}) & \xrightarrow{\text{div}} & [L_0^2]^3 & \longrightarrow & 0. \end{array}$$

In (2.7) and (2.8), the algebraic operators $-\text{mskw}$, \mathcal{S} , and 2vskw are indeed maps between the spaces in the diagrams. This is due to the fact that these maps (anti)commute with the differential operators ∇ , curl , and div . The same argument holds for partial boundary conditions when we impose Dirichlet conditions only on Γ_D . In this case, we need a slight modification in (2.8): the last space is $[L_0^2]^3$ is the entire boundary is Dirichlet, i.e., $\Gamma_D = \partial\Omega$. Otherwise we use $[L^2]^3$.

The following observation relates the twisted complex with Cosserat elasticity.

Lemma 1. *Let C be the material tensor incorporating C_1 and C_2 in (2.1). Then the Cosserat energy (2.2) is a Hodge-Laplacian in the C -weighted inner product, i.e.,*

$$(d_V^0(u, \omega), d_V^0(u, \omega))_C - \int_{\Omega} (\langle f_u, u \rangle + \langle f_{\omega}, \omega \rangle) dx = \mathcal{E}^{\text{Cosserat}}(u, \omega).$$

2.2. Primal formulation for Cosserat and couple stress limit. In this section we derive and discuss the primal formulations for Cosserat elasticity and the couple stress problem.

2.2.1. Primal formulation. Let $H_{\Gamma}^1(\Omega) = \{u \in H^1(\Omega) : \text{tr } u = 0 \text{ on } \Gamma\}$ denote the set of H^1 functions, with zero boundary conditions on $\Gamma \subset \partial\Omega$ and $H^{1/2}(\Gamma)$ the trace space of $H_{\Gamma}^1(\Omega)$. We denote with $H^{-1}(\Omega)$ and $H^{-1/2}(\Gamma)$ the dual spaces of $H_{\Gamma}^1(\Omega)$ and $H^{1/2}(\Gamma)$, respectively. The *primal variation formulation* of (2.3), cf. (2.2) and Lemma 1, reads as follows.

Problem 1 (Primal formulation). *Find $(u, \omega) \in [H^1(\Omega)]^3 \times [H^1(\Omega)]^3$ such that $u = u_D$ and $\omega = \omega_D$ on Γ_D and for all $(v, \xi) \in [H_{\Gamma_D}^1(\Omega)]^3 \times [H_{\Gamma_D}^1(\Omega)]^3$ there holds*

$$(2.9) \quad a((u, \omega), (v, \xi)) = f(v, \xi),$$

where

$$(2.10a) \quad a((u, \omega), (v, \xi)) := \int_{\Omega} (\langle \nabla u - \text{mskw } \omega, \nabla v - \text{mskw } \xi \rangle_{C_1} + \langle \nabla \omega, \nabla \xi \rangle_{C_2}) dx,$$

$$(2.10b) \quad f(v, \xi) := \int_{\Omega} (\langle f_u, v \rangle + \langle f_{\omega}, \xi \rangle) dx + \int_{\Gamma_N} (\langle g_u, v \rangle + \langle g_{\omega}, \xi \rangle) ds.$$

Lemma 2 (Well-posedness). *Let $|\Gamma_D| > 0$ have positive measure, $u_D, \omega_D \in H^{1/2}(\Gamma_D)$, $f_u, f_{\omega} \in [H^{-1}(\Omega)]^3$, and $g_u, g_{\omega} \in [H^{-1/2}(\Gamma_N)]^3$. Then Problem 1 has a unique solution $(u, \omega) \in [H^1(\Omega)]^3 \times [H^1(\Omega)]^3$ and there holds the stability estimate*

$$\|u\|_{H^1(\Omega)} + \|\omega\|_{H^1(\Omega)} \leq C \left(\|f_u\|_{H^{-1}(\Omega)} + \|f_{\omega}\|_{H^{-1}(\Omega)} + \|g_u\|_{H^{-1/2}(\Gamma_N)} + \|g_{\omega}\|_{H^{-1/2}(\Gamma_N)} \right),$$

where the constant $C > 0$ depends especially on the Lamé parameter λ , the Cosserat coupling constant μ_c , and the aspect ratio of the domain Ω .

Proof. Follows by Lax-Milgram Lemma using Korn type inequalities (cf. Remark 1). \square

The lack of robustness in the aspect ratio origins from the Korn inequality. For nearly incompressible materials the Lamé parameter λ goes to infinity. In this work the Cosserat coupling constant is of special interest for us. Its limit $\mu_c \rightarrow \infty$ enforces the equality $1/2 \text{curl } u = \omega$, cf. (2.2).

2.2.2. Lagrange finite elements. Let \mathcal{T} be a triangulation of the three-dimensional domain Ω consisting of (possibly polynomially curved) tetrahedra. Denote for $T \in \mathcal{T}$ the set of polynomials up to order k by $\mathcal{P}^k(T)$. Then $\mathcal{P}^k(\mathcal{T}) = \Pi_{T \in \mathcal{T}} \mathcal{P}^k(T)$ is the set of all elementwise polynomials of order k without any continuity assumption over element interfaces.

We define the scalar-valued *Lagrangian* finite element space as H^1 -conforming subspace by

$$\begin{aligned} \text{Lag}^k &:= \{u_h \in \mathcal{P}^k(\mathcal{T}) : u_h \text{ is continuous}\} = \mathcal{P}^k(\mathcal{T}) \cap C^0(\Omega) \subset H^1(\Omega), \\ \text{Lag}_{\Gamma}^k &:= \{u_h \in \text{Lag}^k : u = 0 \text{ on } \Gamma\} \subset H_{\Gamma}^1(\Omega) \end{aligned}$$

and its vector-valued version $\mathbf{Lag}^k := [\text{Lag}^k]^3$.

A straight forward approach to discretize (2.9) is to use Lagrangian finite elements for both the displacement u and the rotation ω . In the following we always assume that the prescribed Dirichlet data u_D and ω_D are traces of the used finite element spaces. The primal discrete formulation reads:

Problem 2 (Primal discretization method). *Let $k \geq 1$ be an integer. Find $(u_h, \omega_h) \in \mathbf{Lag}^k \times \mathbf{Lag}^k$ such that $u_h = u_D$ and $\omega_h = \omega_D$ on Γ_D and for all $(v_h, \xi_h) \in \mathbf{Lag}_{\Gamma_D}^k \times \mathbf{Lag}_{\Gamma_D}^k$*

$$(2.11) \quad a((u_h, \omega_h), (v_h, \xi_h)) = f(v_h, \xi_h),$$

where $a(\cdot, \cdot)$ and $f(\cdot, \cdot)$ are defined as in (2.10).

Well-posedness of (2.11) follows directly from the continuous level due to the conforming discretization approach $\mathbf{Lag}^k \subset H^1(\Omega)$. Using Cea's Lemma we directly obtain the quasi-best approximation of the finite element solution and a-priori convergence estimates in terms of the mesh-size h . The constant $C = C(\mu_c, \lambda, \Omega)$, however, depends on the Cosserat coupling constant μ_c , Lamé parameter λ , and due to Korn's inequality on the aspect ratio of the domain Ω

$$\|(u_h, \omega_h) - (u, \omega)\|_{H^1 \times H^1} \leq C \inf_{(v_h, \xi_h) \in \mathbf{Lag}^k \times \mathbf{Lag}^k} \|(v_h, \xi_h) - (u, \omega)\|_{H^1 \times H^1} \leq C h^k (|u|_{H^{k+1}} + |\omega|_{H^{k+1}}).$$

As we will demonstrate in Section 5 the primal method suffers from locking when $\mu_c \rightarrow \infty$.

2.2.3. Couple stress formulation. In the formal limit $\mu_c \rightarrow \infty$ we can eliminate ω by u via $1/2 \operatorname{curl} u = \omega$. This yields the following *couple stress problem*. As common for fourth-order problems we can additionally to u also prescribe boundary conditions on parts of its derivative. The corresponding Dirichlet boundaries are denoted by Γ_D and $\Gamma_D^{\operatorname{curl}}$, respectively. Further, we denote with $(v)_t$ the tangential part of a vector v .

Problem 3 (Couple stress). *Let Dirichlet data u_D and ω_D , and the forces $f_u, f_\omega, g_u, g_\omega$ be given. Find $u \in H^1(\operatorname{curl}, \Omega) := \{u \in [H^1(\Omega)]^3 : \operatorname{curl} u \in [H^1(\Omega)]^3\}$ such that $u = u_D$ on Γ_D and $(\operatorname{curl} u)_t = (\operatorname{curl} u_D)_t$ on $\Gamma_D^{\operatorname{curl}}$ and for all $v \in H^1(\operatorname{curl}, \Omega)$ with $v = 0$ on Γ_D and $(\omega_D)_t = 0$ on $\Gamma_D^{\operatorname{curl}}$*

$$(2.12) \quad \begin{aligned} & \int_{\Omega} (\langle \operatorname{sym} \nabla u, \operatorname{sym} \nabla v \rangle_{\mathbb{C}} + 1/4 \langle \nabla \operatorname{curl} u, \nabla \operatorname{curl} v \rangle_{C_2}) \, dx \\ &= \int_{\Omega} (\langle f_u, v \rangle + \langle f_\omega, 1/2 \operatorname{curl} v \rangle) \, dx + \int_{\partial\Omega} (\langle g_u, v \rangle + \langle g_\omega, 1/2 \operatorname{curl} v \rangle) \, ds \end{aligned}$$

with corresponding energy functional

$$\begin{aligned} \mathcal{E}^{\text{CoupleStress}}(u) &= \frac{1}{2} \int_{\Omega} (\|\operatorname{sym} \nabla u\|_{\mathbb{C}}^2 + 1/4 \|\nabla \operatorname{curl} u\|_{C_2}^2) \, dx - \int_{\Omega} (\langle f_u, u \rangle + \langle f_\omega, 1/2 \operatorname{curl} u \rangle) \, dx \\ &\quad - \int_{\partial\Omega} (\langle g_u, u \rangle + \langle g_\omega, 1/2 \operatorname{curl} u \rangle) \, ds \rightarrow \min_u. \end{aligned}$$

Note, that (2.12) is a fourth order minimization problem, similar to the Kirchhoff–Love plate, requiring H^2 -regularity of the displacement field u . For the strong form including general boundary conditions of the couple stress problem, we introduce the elasticity stress tensor $\sigma = \mathbb{C}(\operatorname{sym} \nabla u)$ and the *couple stress* tensor $m = C_2(1/2 \nabla \operatorname{curl} u)$. Then, cf. e.g. [41, 14],

$$(2.13a) \quad -\operatorname{div}(\sigma) - 1/2 \operatorname{curl}(\operatorname{div} m - f_\omega) = f_u \quad \text{in } \Omega,$$

$$(2.13b) \quad u = u_D \quad \text{on } \Gamma_D, \quad \sigma_n + 1/2 n \times (\operatorname{div} m - \nabla(m_{nn}) + f_\omega) = g_u - 1/2 n \times \nabla(g_{\omega,n}) \quad \text{on } \Gamma_N,$$

$$(2.13c) \quad (\operatorname{curl} u)_t = (\operatorname{curl} u_D)_t \quad \text{on } \Gamma_D^{\operatorname{curl}}, \quad m_{nt} = g_{\omega,t} \quad \text{on } \Gamma_N^{\operatorname{curl}}.$$

If the boundary is non-smooth, i.e., there exist sharp edges E , an additional jump condition appears

$$(2.13d) \quad u_{t_E} = u_{D,t_E} \quad \text{or} \quad 1/2((m_{nn})_+ - (m_{nn})_-) = 1/2((g_{\omega,n})_+ - (g_{\omega,n})_-) \quad \text{on } E,$$

where t_E denotes the tangent vector of the edge E and $(\cdot)_\pm$ indicates from which facet adjacent to the edge the quantity gets evaluated. This kind of jump condition appears also for Kirchhoff–Love plates, see e.g. [19].

Using mixed methods the H^2 regularity, which would require e.g. the use of C^1 -conforming finite elements, can be relaxed as shown in Problem 5 and Section 3.3 below. Further, note that the α micropolar modulus parameter is indeterminate for the couple stress problem. By $\text{tr}(\nabla \text{curl } u) = \text{div curl } u = 0$ there holds with (2.1b)

$$(2.14) \quad \begin{aligned} C_2(\nabla \text{curl } u) &= (\gamma + \beta) \text{sym}(\nabla \text{curl } u) + \alpha \text{tr}(\nabla \text{curl } u)I + (\gamma - \beta) \text{skw}(\nabla \text{curl } u) \\ &= (\gamma + \beta) \text{sym}(\nabla \text{curl } u) + (\gamma - \beta) \text{skw}(\nabla \text{curl } u). \end{aligned}$$

3. MIXED TDNNS AND MCS FORMULATIONS FOR COSSERAT ELASTICITY AND COUPLE STRESS

The key idea for achieving robustness with μ_c in discretization is that *the space of the rotation variable w should be large enough to contain $\text{mskw}^\dagger \circ \nabla = \text{vskw} \circ \nabla = \text{curl}$ of the space of the displacement u , where mskw^\dagger is the pseudo-inverse of mskw (see (3.1))*

$$(3.1) \quad \begin{array}{c} \begin{array}{ccc} u & \xrightarrow{\nabla} & \\ & \nearrow -\text{mskw} & \\ \omega & \xrightarrow{\nabla} & m'. \end{array} \end{array}$$

We start with a natural choice $u \in [H^1(\Omega)]^3$ (correspondingly, the Lagrange space on the discrete level). Then $\text{curl } u \in \text{curl}([H^1(\Omega)]^3) \subset H(\text{div})$ (correspondingly, $\text{curl } u$ is in the Raviart-Thomas finite element space on the discrete level). This motivates us to use the $H(\text{div})$ space for w . Then ∇w is in a weak H^{-1} -based Sobolev space (a Dirac delta on the discrete level). We need to introduce the *couple stress* tensor $m = C_2(\nabla w)$ in a proper space to accommodate the pair $\langle \nabla w, m \rangle$. We used the notation m' in (3.1) to indicate that it is in the dual space. In this case, the choice of continuous and discrete spaces for m coincides with the *mass conserving mixed stress (MCS)* method for Stokes equations [24]. Therefore we refer to this formulation as the *MCS method*. Note, that m is not necessarily symmetric.

Although the above idea fixes the dependence on μ_c , since we choose $u \in [H^1(\Omega)]^3$ as the displacement formulation like in classical elasticity, the numerical scheme still suffers from standard volume and shear locking in elasticity. This inspires us to run the above idea starting with $u \in H(\text{curl})$, mimicking the *tangential-displacement normal-normal-stress (TDNNS)* method for elasticity, which was also used for linear elasticity [42] and Reissner–Mindlin plates [44]. Now ∇u is also a distribution and we define the *elasticity stress* tensor $\sigma = \mathcal{C}(\text{sym } \nabla u)$ to evaluate ∇u . The stresses are settled in specific matrix-valued function and finite element spaces introduced in the following sections.

The introduction of σ and m leads to a mixed scheme. We remark that here the idea leading to mixed formulations is different from [7], which explicitly used the last two spaces in the twisted de Rham complex, mimicking the formulation for the mixed Poisson problem.

3.1. Continuous setting. For matrix fields, we use the convention that differential operators act row-wise. We define the vector-valued function spaces

$$\begin{aligned} H(\text{curl}) &:= \{u \in [L^2(\Omega)]^3 : \text{curl } u \in [L^2(\Omega)]^3\}, & H(\text{div}) &:= \{u \in [L^2(\Omega)]^3 : \text{div } u \in L^2(\Omega)\}, \\ H_0(\text{curl}) &:= \{u \in H(\text{curl}) : \text{tr}_t u = 0 \text{ on } \partial\Omega\}, & H_0(\text{div}) &:= \{u \in H(\text{div}) : \text{tr}_n u = 0 \text{ on } \partial\Omega\}, \end{aligned}$$

where tr_t and tr_n denote, respectively, the tangential and normal trace operators, which for continuous u reads $\text{tr}_t u = u \times n$ and $\text{tr}_n u = \langle u, n \rangle$. For simplicity of presentation, we focus in this section on the boundary conditions corresponding to (2.8), i.e., we impose $u = \omega = 0$ on the boundary.

Following [24, 42], we define the following matrix-valued function spaces

$$\begin{aligned}
 H(\operatorname{curl} \operatorname{div}, \mathbb{R}^{3 \times 3}) &:= \{m \in [L^2(\Omega)]^{3 \times 3} : \operatorname{curl} \operatorname{div} m \in [H^{-1}(\Omega)]^3\} \\
 (3.2) \quad &= \{m \in [L^2(\Omega)]^{3 \times 3} : \operatorname{div} m \in H^{-1}(\operatorname{curl})\} = \{m \in [L^2(\Omega)]^{3 \times 3} : \operatorname{div} m \in H_0(\operatorname{div})^*\}, \\
 H(\operatorname{div} \operatorname{div}, \mathbb{R}_{\operatorname{sym}}^{3 \times 3}) &:= \{\sigma \in [L^2(\Omega)]_{\operatorname{sym}}^{3 \times 3} : \operatorname{div} \operatorname{div} \sigma \in H^{-1}(\Omega)\} \\
 (3.3) \quad &= \{\sigma \in [L^2(\Omega)]_{\operatorname{sym}}^{3 \times 3} : \operatorname{div} \sigma \in H^{-1}(\operatorname{div})\} = \{\sigma \in [L^2(\Omega)]_{\operatorname{sym}}^{3 \times 3} : \operatorname{div} \sigma \in H_0(\operatorname{curl})^*\},
 \end{aligned}$$

where we used that the dual space $H_0(\operatorname{div})^*$ of $H_0(\operatorname{div})$ is $H^{-1}(\operatorname{curl}) = \{u \in [H^{-1}(\Omega)]^3 : \operatorname{curl} u \in [H^{-1}(\Omega)]^3\}$ and analogously that $H_0(\operatorname{curl})^* = H^{-1}(\operatorname{div})$. Note that the notation is different from some contexts in literature where the spaces $H(\operatorname{curl} \operatorname{div}, \mathbb{R}^{3 \times 3})$ and $H(\operatorname{div} \operatorname{div}, \mathbb{R}_{\operatorname{sym}}^{3 \times 3})$ contains L^2 fields with their second derivatives in L^2 instead of H^{-1} .

The first space (3.2) represents the stress space on the continuous level of the MCS method for Stokes equations. Due to its definition, the duality-pairing

$$(3.4) \quad \langle \operatorname{div} m, \omega \rangle_{H(\operatorname{div})^*} := \langle \operatorname{div} m, \omega \rangle_{H_0(\operatorname{div})^* \times H_0(\operatorname{div})} = -\langle \nabla \omega, m \rangle_{H(\operatorname{curl} \operatorname{div})^* \times H(\operatorname{curl} \operatorname{div})}$$

is well-defined for all $m \in H(\operatorname{curl} \operatorname{div}, \mathbb{R}^{3 \times 3})$ and $\omega \in H_0(\operatorname{div})$. Space (3.3) is used for the moment stress tensor in the Hellan-Herrmann-Johnson (HHJ) [27, 28, 31] method and the elasticity stress tensor in the TDNNS method for linear elasticity and Reissner-Mindlin plates. Analogously, the following duality-pairing is well-defined for all $\sigma \in H(\operatorname{div} \operatorname{div}, \mathbb{R}_{\operatorname{sym}}^{3 \times 3})$ and $u \in H_0(\operatorname{curl})$

$$(3.5) \quad \langle \operatorname{div} \sigma, u \rangle_{H(\operatorname{curl})^*} := \langle \operatorname{div} \sigma, u \rangle_{H_0(\operatorname{curl})^* \times H_0(\operatorname{curl})} = -\langle \nabla u, \sigma \rangle_{H(\operatorname{div} \operatorname{div})^* \times H(\operatorname{div} \operatorname{div})}.$$

We propose the following two mixed formulations for Cosserat elasticity.

Problem 4 (MCS and TDNNS mixed formulations for linear Cosserat elasticity). *Find $(u, \omega, m) \in [H_0^1(\Omega)]^3 \times H_0(\operatorname{div}) \times H(\operatorname{curl} \operatorname{div}, \mathbb{R}^{3 \times 3})$ solving the Lagrangian*

$$(3.6) \quad \mathcal{L}^m(u, \omega, m) = \frac{1}{2} \int_{\Omega} (\|\nabla u - \operatorname{mskw} \omega\|_{C_1}^2 - \|m\|_{C_2^{-1}}^2) dx - \langle \operatorname{div} m, \omega \rangle_{H(\operatorname{div})^*} - f(u, \omega, m) \rightarrow \min_{u, \omega} \max_m.$$

Find $(u, \omega, m, \sigma) \in H_0(\operatorname{curl}) \times H_0(\operatorname{div}) \times H(\operatorname{curl} \operatorname{div}, \mathbb{R}^{3 \times 3}) \times H(\operatorname{div} \operatorname{div}, \mathbb{R}_{\operatorname{sym}}^{3 \times 3})$ solving the Lagrangian

$$(3.7) \quad \mathcal{L}^{m, \sigma}(u, \omega, \sigma, m) = \frac{1}{2} \int_{\Omega} \left(-\|\sigma\|_{\mathcal{C}^{-1}}^2 + 2\mu_c \|^{1/2} \operatorname{curl} u - \omega\|^2 - \|m\|_{C_2^{-1}}^2 \right) dx - \langle \operatorname{div} \sigma, u \rangle_{H(\operatorname{curl})^*} - \langle \operatorname{div} m, \omega \rangle_{H(\operatorname{div})^*} - f(u, \omega, m, \sigma) \rightarrow \min_{u, \omega} \max_{m, \sigma}.$$

The inverse of C_2 is given e.g. by

$$C_{2, \operatorname{pw}}^{-1}(m) = \frac{1}{\beta + \gamma} \operatorname{dev} \operatorname{sym} m + \frac{1}{3(3\alpha + \beta + \gamma)} \operatorname{tr} m I + \frac{1}{\gamma - \beta} \operatorname{skw} m = \frac{1}{\gamma} m,$$

cf. Remark 1, and the inverse of \mathcal{C} , called compliance tensor, reads

$$\mathcal{C}^{-1}(\sigma) = \frac{1}{2\mu} \operatorname{dev} \operatorname{sym} \sigma + \frac{1}{3(3\lambda + 2\mu)} \operatorname{tr} \sigma I.$$

The MCS formulation (3.6) is based on the following diagram:

$$\begin{array}{ccc}
 [H_0^1(\Omega)]^3 & \xrightarrow{\nabla} & \text{---} \\
 & \searrow -\operatorname{mskw} & \\
 H_0(\operatorname{div}) & \xrightarrow{\nabla} & H(\operatorname{curl} \operatorname{div}, \mathbb{R}^{3 \times 3})^*
 \end{array}, \quad
 \begin{array}{ccc}
 u & \xrightarrow{\nabla} & \text{---} \\
 & \searrow -\operatorname{mskw} & \\
 \omega & \xrightarrow{\nabla} & m',
 \end{array}$$

where we used the notation m' to indicate that m is introduced in the dual space. The TDNNS-MCS formulation (3.7) is based on the diagram

$$\begin{array}{ccc} H_0(\text{curl}) & \xrightarrow{\nabla} & H(\text{div div}, \mathbb{R}_{\text{sym}}^{3 \times 3})^* \times [L^2(\Omega)]_{\text{skw}}^{3 \times 3} \\ & \nearrow -\text{mskw} & \\ H_0(\text{div}) & \xrightarrow{\nabla} & H(\text{curl div}, \mathbb{R}^{3 \times 3})^* \end{array}, \quad \begin{array}{ccc} u & \xrightarrow{\nabla} & \sigma' \\ & \nearrow -\text{mskw} & \\ \omega & \xrightarrow{\nabla} & m'. \end{array}$$

Similarly, we use σ' and m' to indicate that σ and m are in the dual spaces.

Taking formally the limit $\mu_c \rightarrow \infty$ in (3.6) yields the following MCS mixed formulation for the couple stress problem:

Problem 5 (MCS method for couple stress problem). *Find $u \in H_0^1(\Omega)$ and $m \in H(\text{curl div}, \mathbb{R}_{\text{dev}}^{3 \times 3})$*

$$(3.8) \quad \mathcal{L}^{\text{CS},m}(u, m) = \frac{1}{2} \int_{\Omega} \left(\|\text{sym } \nabla u\|_{\mathbb{C}}^2 - \|m\|_{C_2^{-1}}^2 \right) dx - \frac{1}{2} \langle \text{div } m, \text{curl } u \rangle_{H(\text{div})^*} - f(u, m).$$

Note that m will always be deviatoric due to $\text{tr}(\nabla \text{curl } u) = \text{div } \text{curl } u = 0$, cf. (2.14).

We recall that in the formal limit $\mu_c \rightarrow \infty$ we establish the constraint

$$(3.9) \quad \frac{1}{2} \text{curl } u = \omega.$$

Thus, a necessary condition to avoid locking later in the finite element computations is that the chosen function spaces can represent (3.9) exactly. In the primal setting (2.9), where $(u, \omega) \in [H^1(\Omega)]^3 \times [H^1(\Omega)]^3$, the constraint is obviously not fulfilled. This indicates that there might occur locking after discretization. The curl of a function in $[H^1(\Omega)]^3$ or $H(\text{curl})$ is in $H(\text{div})$. Hence, seeking for the rotation field ω in $H(\text{div})$ is a natural choice and enables to fulfill the constraint (3.9) exactly. This indicating that the mixed formulations (3.6) and (3.7) have the potential to be robust with respect to the Cosserat coupling constant μ_c , if the discretization is done carefully.

The use of the TDNNS formulation in (3.7) yields further beneficial properties to the method: It becomes more robust with respect to anisotropic domains with large aspect ratio, i.e., avoids shear locking [43], and in the discrete setting by adding a stabilization term it will be free of volumetric locking when $\lambda \rightarrow \infty$ in the incompressible limit [42].

3.2. Finite element spaces. We define several vector- and matrix-valued finite element spaces that will be used below. The *Raviart–Thomas* (RT) [46] and the *Brezzi–Douglas–Marini* (BDM) elements [10] are used for discretizing $H(\text{div})$ and the *Nédélec* elements (of first and second kind) [34] for $H(\text{curl})$. They fit in the de Rham complexes [2, 3, 4]. For simplicity of presentation, we only use the RT and the Nédélec element of the second kind below, defined by

$$\text{RT}^k := \{u \in H(\text{div}) : \forall T \in \mathcal{T} \, u|_T = a + bx, a \in [\mathcal{P}^k(T)]^3, b \in \tilde{\mathcal{P}}^k(T)\} \subsetneq [\mathcal{P}^k(\mathcal{T})]^3 \cap C^n(\mathcal{T}) \subset H(\text{div}),$$

$$\text{RT}_{\Gamma}^k := \{u_h \in \text{RT}^k : \langle u_h, n \rangle = 0 \text{ on } \Gamma\} \subset H_{\Gamma}(\text{div}),$$

$$\text{Ned}_{II}^k := \{u \in H(\text{curl}) : u|_T \in [\mathcal{P}^k(T)]^3, \forall T \in \mathcal{T}\} = [\mathcal{P}^k(\mathcal{T})]^3 \cap C^t(\mathcal{T}) \subset H(\text{curl}),$$

$$\text{Ned}_{II,\Gamma}^k := \{u_h \in \text{Ned}_{II}^k : u_h \times n = 0 \text{ on } \Gamma\} \subset H_{\Gamma}(\text{curl}),$$

where the set of elementwise homogeneous polynomials of order k is denoted by $\tilde{\mathcal{P}}(\mathcal{T})$, $C^t(\mathcal{T})$ indicates that the tangential components of the fields are continuous across the facets of the cells, and $C^n(\mathcal{T})$ indicates the continuity of the normal component. In the lowest order cases, RT^0 consists of facet-based shape function and Ned_{II}^1 consists of edge-based basis functions.

We have the following finite element de Rham complex for $k \geq 3$:

$$0 \longrightarrow \text{Lag}^k \xrightarrow{\nabla} \text{Ned}_{II}^{k-1} \xrightarrow{\text{curl}} \text{RT}^{k-2} \xrightarrow{\text{div}} \mathcal{P}^{k-3}(\mathcal{T}) \longrightarrow 0.$$

The MCS element [24] has tangential-normal continuity and is a slightly non-conforming subspace of $H(\text{curl div}, \mathbb{R}^{3 \times 3})$

$$(3.10) \quad \text{MCS}^k := \{\sigma_h \in [\mathcal{P}^k(\mathcal{T})]^{3 \times 3} : n_F \times (\sigma_h n_F) \text{ is continuous across all facets } F \in \mathcal{F}\}.$$

The TDNNS [42] and HHJ methods discretizes the arising stress tensor using symmetric piecewise polynomials with normal-normal continuity. We denote this space by

$$\text{HHJ}^k := \{\sigma_h \in [\mathcal{P}^k(\mathcal{T})]_{\text{sym}}^{3 \times 3} : \sigma_{h, n_F n_F} := \langle \sigma_h n_F, n_F \rangle \text{ is continuous across all facets } F \in \mathcal{F}\},$$

which is a slightly non-conforming subspace of $H(\text{div div}, \mathbb{R}_{\text{sym}}^{3 \times 3})$. The definitions of MCS_Γ^k and HHJ_Γ^k are done analogously to RT_Γ^k and $\text{Ned}_{II, \Gamma}^k$ by forcing the tangential-normal and normal-normal trace to be zero on Γ , respectively.

The above spaces are characterized by local shape functions and interelement continuity. Possible degrees of freedom for tetrahedral elements can be found in the references above.

The following simple observation shows that the constraint (3.9) is also fulfilled in the discrete setting.

Lemma 3. *Let $u \in \mathbf{Lag}_\Gamma^k$ or $u \in \text{Ned}_{II, \Gamma}^k$. Then $\text{curl } u \in \text{RT}_\Gamma^{k-1}$ and $\text{curl } u \in \text{RT}_\Gamma^{k-1}$.*

Proof. The claim follow by noting that $\text{curl } u$ is normal continuous for Lagrangian and Nédélec elements and fulfills the zero boundary conditions. \square

3.3. Mass conserving mixed stress (MCS) formulation for rotational part. For $u_h \in \mathbf{Lag}^k$ its curl is in RT^{k-1} . Therefore, setting $\omega_h \in \text{RT}^{k-1}$ enables to satisfy the constraint $\omega_h = 1/2 \text{curl } u_h$ exactly, such that, as we will prove in Section 4, the method will be locking free for $\mu_c \rightarrow \infty$.

3.3.1. MCS method for Cosserat elasticity. In [24] it is shown that for $\omega_h \in \text{RT}^{k-1}$ and $m_h \in \text{MCS}^{k-1}$ the duality pairing (3.4) has the explicit mesh dependent form

$$(3.11) \quad \begin{aligned} \langle \nabla \omega_h, m_h \rangle_{H(\text{curl div})^*} &= \sum_{T \in \mathcal{T}} \left(\int_T \langle \nabla \omega_h, m_h \rangle dx - \int_{\partial T} \langle \omega_{h,t}, m_{h,nt} \rangle ds \right) \\ &= - \sum_{T \in \mathcal{T}} \left(\int_T \langle \omega_h, \text{div } m_h \rangle dx - \int_{\partial T} \omega_{h,n} m_{h,nn} ds \right) = - \langle \text{div } m_h, \omega_h \rangle_{H(\text{div})^*}. \end{aligned}$$

Above, n is the outer unit normal vector of element T and $\omega_{h,t} := (I - n \otimes n) \omega_h$ denotes the projection onto the tangent space. If we reorder the boundary integrals in (3.11) as jumps over facets, we recognize that always a continuous term hits a discontinuous one

$$\sum_{T \in \mathcal{T}} \int_{\partial T} \omega_{h,n} m_{h,nn} ds = \sum_{F \in \mathcal{F}} \int_F \omega_{h,n} \llbracket m_{h,nn} \rrbracket ds, \quad \sum_{T \in \mathcal{T}} \int_{\partial T} \langle \omega_{h,t}, m_{h,nt} \rangle ds = \sum_{F \in \mathcal{F}} \int_F \langle \llbracket \omega_{h,t} \rrbracket, m_{h,nt} \rangle ds,$$

where $\llbracket \cdot \rrbracket$ is the jump over facets. We pose the *MCS discretization for Cosserat elasticity* as follows.

Problem 6. *Let $k \geq 1$ be an integer. Find $(u_h, \omega_h, m_h) \in \mathbf{Lag}^k \times \text{RT}^{k-1} \times \text{MCS}^{k-1}$ such that $u_h = u_D$ and $\omega_{h,n} = \omega_{D,n}$ on Γ_D , $m_{h,t} = g_{\omega,t}$ on Γ_N , and for all $(v_h, \xi_h, \Psi_h) \in \mathbf{Lag}_{\Gamma_D}^k \times \text{RT}_{\Gamma_D}^{k-1} \times \text{MCS}_{\Gamma_N}^{k-1}$,*

$$(3.12a) \quad a(m_h, \Psi_h) + b(\Psi_h, (u_h, \omega_h)) = g(\Psi_h),$$

$$(3.12b) \quad b(m_h, (v_h, \xi_h)) - c((u_h, \omega_h), (v_h, \xi_h)) = -f(v_h, \xi_h),$$

where

$$(3.13a) \quad a(m, \Psi) := \int_{\Omega} \langle m, \Psi \rangle_{C_2^{-1}} dx, \quad b(\Psi, (u, \omega)) := \langle \omega, \operatorname{div} \Psi \rangle_{H(\operatorname{div})^*},$$

$$(3.13b) \quad c((u, \omega), (v, \xi)) := \int_{\Omega} 2\mu_c \langle 1/2 \operatorname{curl} u - \omega, 1/2 \operatorname{curl} v - \xi \rangle dx,$$

$$(3.13c) \quad f(v, \xi) := \int_{\Omega} (\langle f_u, v \rangle + \langle f_{\omega}, \xi \rangle) dx + \int_{\Gamma_N} (\langle g_u, v \rangle + g_{\omega, n} \xi_n) ds, \quad g(\Psi) := \int_{\Gamma_D} \langle \Psi_{nt}, \omega_{D, t} \rangle ds.$$

The numerical analysis of Problem 6 will follow from the (more involved) analysis of the method presented in the next section, cf. Corollary 1. Note, that the Dirichlet and Neumann boundary conditions ω_D , g_{ω} are treated half-half as essential and natural boundary condition. This comes from the shared regularity between the rotation ω_h and couple stress tensor m_h . The change of essential and natural boundary conditions between primal and mixed formulations are classical in mixed methods, see e.g. [6].

By construction, the couple stress space MCS for m_h can easily be changed between full matrices and deviatoric ones [24]. To incorporate symmetry conditions on m_h an additional Lagrange multiplier enforcing weak symmetry can be introduced [23, 22]. In this work, however, we will restrict our analysis to the case of full matrices and refer to the cited literature for the other cases.

Problem 6 has the form of a saddle-point problem, which would lead to an indefinite stiffness matrix after assembling. We can apply hybridization techniques to overcome this problem [6]. For the sake of simplicity, however, we refer to the literature for details [23].

3.3.2. MCS method for couple stress problem. One obtains directly a mixed finite element method for the couple stress problem (3.8) circumventing the problem of having a fourth order problem:

Problem 7. Find $(u_h, m_h) \in \mathbf{Lag}^k \times \text{MCS}^{k-1}$ solving the Lagrangian

$$\mathcal{L}_{\text{MCS}}^{\text{CS}}(u_h, m_h) = \frac{1}{2} \int_{\Omega} \left(\|\operatorname{sym} \nabla u_h\|_{\mathbb{C}}^2 - \|m_h\|_{C_2^{-1}}^2 \right) dx - \frac{1}{2} \langle \operatorname{div} m_h, \operatorname{curl} u_h \rangle_{H(\operatorname{div})^*} - f(u_h, m_h).$$

The analysis of the couple stress problem with MCS elements is topic of future research. We note, that in [13] the quad-curl problem has been investigated with MCS elements, where instead of the elasticity stress the constraint $\operatorname{div} u = 0$ is used and Nédélec elements for u_h are considered.

3.4. Tangential-displacement normal-normal-stress (TDNNS) formulation for displacement part. Due to Korn's inequality the standard elasticity formulation is not robust with respect to anisotropic structures. Further, it is well-known that locking can occur in the nearly incompressible regime when $\lambda \rightarrow \infty$. The TDNNS method [42] is robust in both cases. We will use it on top of the previously introduced MCS method to discretize the elasticity part. To this end, the displacement fields are settled in the Nédélec space, $u_h \in \text{Ned}_{II}^k$. There still holds $\operatorname{curl} u_h \in \text{RT}^{k-1}$, cf. Lemma 3, such that constraint (3.9) holds when using $\omega_h \in \text{RT}^{k-1}$.

For $u_h \in \text{Ned}_{II}^k$ and $\sigma_h \in \text{HHJ}^k$ the duality pairing (3.5) is well-defined and takes the explicit form [42], cf. (3.11),

$$\langle \operatorname{div} \sigma_h, u_h \rangle_{H(\operatorname{curl})^*} = \sum_{T \in \mathcal{T}} \left(\int_T \langle u_h, \operatorname{div} \sigma_h \rangle dx + \int_{\partial T} \langle u_{h, t}, \sigma_{h, nt} \rangle ds \right).$$

We define the *TDNNS-MCS discretization method for linear Cosserat elasticity* as follows.

Problem 8. Let $k \geq 1$ be an integer. Find $(u_h, \omega_h, m_h, \sigma_h) \in \text{Ned}_{II}^k \times \text{RT}^{k-1} \times \text{MCS}^{k-1} \times \text{HHJ}^k$ such that $u_{h, t} = u_{D, t}$ and $\omega_{h, n} = \omega_{D, n}$ on Γ_D , $m_{h, nt} = g_{\omega, t}$ and $\sigma_{h, nn} = g_{u, n}$ on Γ_N and for all

$$(v_h, \xi_h, \Psi_h, \Theta_h) \in \text{Ned}_{II, \Gamma_D}^k \times \text{RT}_{\Gamma_D}^{k-1} \times \text{MCS}_{\Gamma_N}^{k-1} \times \text{HHJ}_{\Gamma_N}^k,$$

$$(3.14a) \quad a((m_h, \sigma_h), (\Psi_h, \Theta_h)) + b((\Psi_h, \Theta_h), (u_h, \omega_h)) = g(\Psi_h, \Theta_h),$$

$$(3.14b) \quad b((m_h, \sigma_h), (v_h, \xi_h)) - c((u_h, \omega_h), (v_h, \xi_h)) = -f(v_h, \xi_h),$$

where $c(\cdot, \cdot)$ is defined as in (3.13b) and

$$\begin{aligned} a((m, \sigma), (\Psi, \Theta)) &:= \int_{\Omega} \left(\langle m, \Psi \rangle_{C_2^{-1}} + \langle \sigma, \Theta \rangle_{C^{-1}} \right) dx, \\ b((\Psi, \Theta), (u, \omega)) &:= \langle \omega, \text{div } \Psi \rangle_{H(\text{div})^*} + \langle u, \text{div } \Theta \rangle_{H(\text{curl})^*}, \\ f(v, \xi) &:= \int_{\Omega} (\langle f_u, v \rangle + \langle f_{\omega}, \xi \rangle) dx + \int_{\Gamma_N} (\langle g_{u,t}, v_t \rangle + g_{\omega,n} \xi_n) ds, \\ g(\Psi, \Theta) &:= \int_{\Gamma_D} (\langle \Psi_{nt}, \omega_{D,t} \rangle + \Theta_{nn} u_{D,n}) ds. \end{aligned}$$

In (3.14), additionally to ω_D and g_{ω} , also u_D and g_u are treated half-half as essential and natural boundary conditions. The system in (u_h, σ_h) has the form of a saddle-point problem, very similar to the TDNNS method. We can again use hybridization techniques to retain a symmetric and positive definite problem, cf. e.g. [6, 38, 42, 55].

4. STABILITY, ERROR ANALYSIS, AND POST-PROCESSING

For the numerical analysis we assume throughout this section that homogeneous Dirichlet boundary conditions are prescribed on the whole boundary to simplify expressions. We emphasize that the extension to Neumann and non-homogeneous boundary conditions is straight-forward.

4.1. Stability. To show that (3.14) is well-posed and robust with respect to the Cosserat coupling constant μ_c we follow the strategy of [44]. First, we add the unknown $\gamma := 2\mu_c(1/2 \text{curl } u - \omega) \in H(\text{div})$ (and $\gamma_h = 2\mu_c(1/2 \text{curl } u_h - \omega_h) \in \text{RT}^{k-1}$), which can be physically interpreted as a *shear stress* quantity. Problem 8 is then equivalent to the following problem:

Problem 9. Let $k \geq 1$ be an integer. Find $(u_h, \omega_h, m_h, \sigma_h, \gamma_h) \in \text{Ned}_{II,0}^k \times \text{RT}_0^{k-1} \times \text{MCS}^{k-1} \times \text{HHJ}^k \times \text{RT}_0^{k-1}$ such that for all $(v_h, \xi_h, \Psi_h, \Theta_h, \delta_h) \in \text{Ned}_{II,0}^k \times \text{RT}_0^{k-1} \times \text{MCS}^{k-1} \times \text{HHJ}^k \times \text{RT}_0^{k-1}$

$$(4.1a) \quad a((m_h, \sigma_h, \gamma_h), (\Psi_h, \Theta_h, \delta_h)) + b((\Psi_h, \Theta_h, \delta_h), (u_h, \omega_h)) = 0,$$

$$(4.1b) \quad b((m_h, \sigma_h, \gamma_h), (v_h, \xi_h)) = -f(v_h, \xi_h),$$

where f is defined as in Problem 8 and

$$(4.2a) \quad a((m, \sigma, \gamma), (\Psi, \Theta, \delta)) := \int_{\Omega} \left(\langle m, \Psi \rangle_{C_2^{-1}} + \langle \sigma, \Theta \rangle_{C^{-1}} + \frac{1}{2\mu_c} \langle \gamma, \delta \rangle \right) dx,$$

$$(4.2b) \quad b((m, \sigma, \gamma), (u, \omega)) := \langle \text{div } \sigma, u \rangle_{H(\text{curl})^*} + \langle \text{div } m, \omega \rangle_{H(\text{div})^*} - \int_{\Omega} \langle 1/2 \text{curl } u - \omega, \gamma \rangle dx.$$

Equivalence follows directly, as we can eliminate γ_h algebraically due to the choice of finite element spaces. So the smaller system should be used for implementation. Nevertheless, it will be useful for proving robustness. First, we prove well-posedness of the proposed discrete mixed problems.

Theorem 1. Problems 8–9 are well-posed and there holds with $\gamma_h = 2\mu_c(1/2 \text{curl } u_h - \omega_h)$ the following stability estimate

$$(4.3) \quad \|m_h\|_{L^2} + \|\sigma_h\|_{L^2} + \|\gamma_h\|_{\Gamma} + \|u_h\|_{V_h} + \|\omega_h\|_{W_h} + \sqrt{\mu_c} \|1/2 \text{curl } u_h - \omega_h\|_{L^2} \leq C(\|f_u\|_{L^2} + \|f_{\omega}\|_{L^2}),$$

where $C > 0$ is a constant independent of μ_c and the norms $\|\cdot\|_\Gamma$, $\|\cdot\|_{V_h}$, and $\|\cdot\|_{W_h}$ are given by

$$\begin{aligned} \|u\|_{V_h}^2 &= \sum_{T \in \mathcal{T}} \|\text{sym } \nabla u\|_{L^2(T)}^2 + \frac{1}{h} \sum_{F \in \mathcal{F}} \|[[u_n]]\|_{L^2(F)}^2, & \|\gamma\|_\Gamma &= \frac{1}{\sqrt{\mu_c}} \|\gamma\|_{L^2}, \\ \|\omega\|_{W_h}^2 &= \sum_{T \in \mathcal{T}} \|\nabla \omega\|_{L^2(T)}^2 + \frac{1}{h} \sum_{F \in \mathcal{F}} \|[[\omega_t]]\|_{L^2(F)}^2. \end{aligned}$$

Proof. We use Brezzi's theorem of mixed saddle point problems [9]. On the product spaces

$$X_h := \text{HHJ}^k \times \text{MCS}^{k-1} \times \text{RT}^{k-1}, \quad Y_h := \text{Ned}_{II}^k \times \text{RT}^{k-1}$$

we define the following parameter depending norms

$$\|(m, \sigma, \gamma)\|_{X_h}^2 = \|m\|_{L^2}^2 + \|\sigma\|_{L^2}^2 + \|\gamma\|_\Gamma^2, \quad \|(u, \omega)\|_{Y_h}^2 = \|u\|_{V_h}^2 + \|\omega\|_{W_h}^2 + \mu_c \|1/2 \text{curl } u - \omega\|_{L^2}^2.$$

We denote the lower and upper limit of the material tensors for $\sigma_h \in \text{HHJ}^k$ and $m_h \in \text{MCS}^{k-1}$ by

$$\underline{c}_1 \|\sigma_h\|^2 \leq \|\sigma_h\|_{\mathbb{C}^{-1}}^2 \leq \bar{c}_1 \|\sigma_h\|^2, \quad \underline{c}_2 \|m_h\|^2 \leq \|m_h\|_{C_2^{-1}}^2 \leq \bar{c}_2 \|m_h\|^2.$$

The continuity of the right-hand side, $|f(v_h, \xi_h)| \leq (\|f_u\|_{L^2} + \|f_\omega\|_{L^2}) \|(v_h, \xi_h)\|_{Y_h}$, is straightforward. Continuity of bilinear form $a(\cdot, \cdot) : X_h \times X_h \rightarrow \mathbb{R}$ follows directly by the Cauchy-Schwarz inequality. For all $(m_h, \sigma_h, \gamma_h), (\Psi_h, \Theta_h, \delta_h) \in X_h$ there holds

$$|a((m_h, \sigma_h, \gamma_h), (\Psi_h, \Theta_h, \delta_h))| \leq 3c_3 \|(m_h, \sigma_h, \gamma_h)\|_{X_h} \|(\Psi_h, \Theta_h, \delta_h)\|_{X_h},$$

with $c_3 = \max\{\bar{c}_1, \bar{c}_2, 1/2\}$. For the continuity of bilinear form $b(\cdot, \cdot) : X_h \times Y_h \rightarrow \mathbb{R}$ we use that

$$\langle \text{div } \sigma_h, u_h \rangle_{H(\text{curl})^*} \leq \bar{c}_T \|\sigma_h\|_{L^2} \|u_h\|_{V_h} \quad \text{and} \quad \langle \text{div } m_h, \omega_h \rangle_{H(\text{div})^*} \leq \bar{c}_M \|m_h\|_{L^2} \|\omega_h\|_{W_h}$$

have been proved in the analysis of the TDNNS [42] and MCS [24] methods. There holds for all $(m_h, \sigma_h, \gamma_h) \in X_h$ and $(u_h, \omega_h) \in Y_h$

$$\begin{aligned} |b((m_h, \sigma_h, \gamma_h), (u_h, \omega_h))| &\leq \bar{c}_T \|\sigma_h\|_{L^2} \|u_h\|_{V_h} + \bar{c}_M \|m_h\|_{L^2} \|\omega_h\|_{W_h} + \sqrt{\mu_c} \|1/2 \text{curl } u_h - \omega_h\|_{L^2} \|\gamma_h\|_\Gamma \\ &\leq 3 \max\{\bar{c}_T, \bar{c}_M, 1\} \|(m_h, \sigma_h, \gamma_h)\|_{X_h} \|(u_h, \omega_h)\|_{Y_h}. \end{aligned}$$

Bilinear form $a(\cdot, \cdot)$ is coercive on the whole space, i.e., there holds for all $(m_h, \sigma_h, \gamma_h) \in X_h$

$$a((m_h, \sigma_h, \gamma_h), (m_h, \sigma_h, \gamma_h)) \geq \underline{c}_1 \|m_h\|_{L^2}^2 + \underline{c}_2 \|\sigma_h\|_{L^2}^2 + 1/2 \|\gamma_h\|_\Gamma^2 \geq \min\{\underline{c}_1, \underline{c}_2, 1/2\} \|(m_h, \sigma_h, \gamma_h)\|_{X_h}^2.$$

We are left to check the Ladyzhenskaya–Babuška–Brezzi (LBB) condition. To this end, let an arbitrary element $(u_h, \omega_h) \in Y_h$ be given. Choose $\tilde{\gamma}_h := -\sqrt{\mu_c} (1/2 \text{curl } u_h - \omega_h)$, and $\tilde{m}_h \in \text{MCS}^{k-1}$ and $\tilde{\sigma}_h \in \text{HHJ}^k$ such that, see [42, 24] for the TDNNS and MCS LBB conditions,

$$\langle \text{div } \tilde{m}_h, \omega_h \rangle_{H(\text{div})^*} \geq \underline{c}_M \|\tilde{m}_h\|_{L^2} \|\omega_h\|_{W_h}, \quad \langle \text{div } \tilde{\sigma}_h, u_h \rangle_{H(\text{curl})^*} \geq \underline{c}_T \|\tilde{\sigma}_h\|_{L^2} \|u_h\|_{V_h}.$$

We note, that the choice of polynomial degree for the trace part of \tilde{m}_h is crucial for the MCS LBB condition, which takes the role of the pressure here. Then, we have

$$\begin{aligned} \sup_{(m_h, \sigma_h, \gamma_h) \in X_h} \frac{b((m_h, \sigma_h, \gamma_h), (u_h, \omega_h))}{\|(m_h, \sigma_h, \gamma_h)\|_{X_h}} &\geq \frac{1}{3} \left(\sup_{m_h \in \text{MCS}^{k-1}} \frac{b((m_h, 0, 0), (u_h, \omega_h))}{\|m_h\|_{L^2}} \right. \\ &\quad \left. + \sup_{\sigma_h \in \text{HHJ}^k} \frac{b((0, \sigma_h, 0), (u_h, \omega_h))}{\|\sigma_h\|_{L^2}} + \sup_{\gamma_h \in \text{RT}^{k-1}} \frac{b((0, 0, \gamma_h), (u_h, \omega_h))}{\|\gamma_h\|_\Gamma} \right) \\ &\geq \frac{1}{3} \left(\frac{\langle \text{div } \tilde{m}_h, \omega_h \rangle_{H(\text{div})^*}}{\|\tilde{m}_h\|_{L^2}} + \frac{\langle \text{div } \tilde{\sigma}_h, u_h \rangle_{H(\text{curl})^*}}{\|\tilde{\sigma}_h\|_{L^2}} + \frac{\sqrt{\mu_c} \|1/2 \text{curl } u_h - \omega_h\|_{L^2}^2}{\|1/2 \text{curl } u_h - \omega_h\|_{L^2}} \right) \\ &\geq \min\{1/3, \underline{c}_M, \underline{c}_T\} \|(u_h, \omega_h)\|_{Y_h}. \end{aligned}$$

By Brezzi's theorem, Problem 9 (and therefore Problem 8) is well-posed and stability estimate (4.3) holds. As all involved constants $\underline{c}_1, \underline{c}_2, \bar{c}_1, \bar{c}_2, \underline{c}_M, \underline{c}_T, \bar{c}_M$, and \bar{c}_T are independent of μ_c the constant C in (4.3) is also independent of μ_c . \square

Some comments are in place. By estimate (4.3) we have shown a robust a-priori estimate with respect to the Cosserat coupling constant μ_c . Further, we obtain that the rotation field ω_h converges to the curl of the displacement u_h as $\mu_c \rightarrow \infty$ with at least a root-convergence

$$\|1/2 \operatorname{curl} u_h - \omega_h\|_{L^2} \leq C/\sqrt{\mu_c}, \quad C \neq C(\mu_c).$$

Remark 2 (Robustness with respect to anisotropic structures and nearly incompressibility). *Throughout the proof, including the cited inequalities, we never used a Korn's inequality, where the resulting constant would depend on the aspect ratio of the domain. This indicates that the discrete methods will be free of shear locking. Nevertheless, a detailed convergence analysis would require hexahedra elements and anisotropic estimates, which are out of scope of this paper. We refer to [43] for an anisotropic analysis for the TDNNS method. In the presented proof the Lamé constant λ enters the coercivity constant of $a(\cdot, \cdot)$. With the stabilization techniques presented in [55] one can, with a different choice of discrete norms, adapt the proof to obtain a constant independent of λ , i.e. robustness in the nearly incompressible limit $\lambda \rightarrow \infty$.*

Before we can prove convergence, we need the following consistency result.

Theorem 2 (Consistency & Galerkin orthogonality). *Problems 6, 8, and 9 are consistent. Assume the exact solution of Cosserat problem (2.9) fulfills the following regularity assumptions*

$$u \in [H^1(\Omega)]^3, \quad \omega \in [H^1(\Omega)]^3, \quad \sigma \in [H^1(\Omega)]^{3 \times 3}, \quad m \in [H^1(\Omega)]^{3 \times 3}.$$

For Problem 9 there holds for all $(u_h, \omega_h, m_h, \sigma_h, \gamma_h) \in \operatorname{Ned}_{II,0}^k \times \operatorname{RT}_0^{k-1} \times \operatorname{MCS}^{k-1} \times \operatorname{HHJ}^k \times \operatorname{RT}^{k-1}$

$$a((m, \sigma, \gamma), (m_h, \sigma_h, \gamma_h)) + b((m_h, \sigma_h, \gamma_h), (u, \omega)) + b((m, \sigma, \gamma), (u_h, \omega_h)) = -f(u_h, \omega_h),$$

where a , b , and f are defined as in (4.2). Further, there holds the following Galerkin orthogonality. Let $(u_h, \omega_h, m_h, \sigma_h, \gamma_h) \in \operatorname{Ned}_{II}^k \times \operatorname{RT}^{k-1} \times \operatorname{MCS}^{k-1} \times \operatorname{HHJ}^k \times \operatorname{RT}^{k-1}$ be the solution of Problem 9. Then for all $(v_h, \xi_h, \Psi_h, \Theta_h, \delta_h) \in \operatorname{Ned}_{II,0}^k \times \operatorname{RT}_0^{k-1} \times \operatorname{MCS}^{k-1} \times \operatorname{HHJ}^k \times \operatorname{RT}^{k-1}$ there holds

$$(4.4) \quad \begin{aligned} & a((m - m_h, \sigma - \sigma_h, \gamma - \gamma_h), (\Psi_h, \Theta_h, \delta_h)) + b((\Psi_h, \Theta_h, \delta_h), (u - u_h, \omega - \omega_h)) \\ & + b((m - m_h, \sigma - \sigma_h, \gamma - \gamma_h), (v_h, \xi_h)) = 0. \end{aligned}$$

Proof. We show consistency with respect to Problem 9. The other cases are shown analogously (see also Corollary 1 for the according adaptations for Problem 6).

Due to the regularity assumptions, there holds $\llbracket m_{nn} \rrbracket = \llbracket \sigma_{nt} \rrbracket = \llbracket u_n \rrbracket = \llbracket \omega_t \rrbracket = 0$, and the duality pairings reduce to L^2 integrals, e.g.,

$$\begin{aligned} \langle \omega_h, \operatorname{div} m \rangle_{H(\operatorname{div})^*} &= \sum_{T \in \mathcal{T}} \int_T \langle \omega_h, \operatorname{div} m \rangle dx - \sum_{F \in \mathcal{F}} \int_F \omega_{h,n} \llbracket m_{nn} \rrbracket ds = \int_{\Omega} \langle \omega_h, \operatorname{div} m \rangle dx, \\ \langle \omega, \operatorname{div} m_h \rangle_{H(\operatorname{div})^*} &= - \sum_{T \in \mathcal{T}} \int_T \langle \nabla \omega, m_h \rangle dx + \sum_{F \in \mathcal{F}} \int_F \langle m_{h,nt}, \llbracket \omega_t \rrbracket \rangle ds = - \int_{\Omega} \langle \nabla \omega, m_h \rangle dx. \end{aligned}$$

Using that for the exact solution there holds $\gamma = 2\mu_c(1/2 \operatorname{curl} u - \omega)$ and with integration by parts

$$\begin{aligned} - \int_{\Omega} \langle 1/2 \operatorname{curl} u_h - \omega_h, \gamma \rangle dx &= -2\mu_c \int_{\Omega} \langle 1/2 \operatorname{curl} u_h - \omega_h, 1/2 \operatorname{curl} u - \omega \rangle dx \\ &= 2\mu_c \int_{\Omega} (\langle 1/2 \operatorname{curl} u - \omega, \omega_h \rangle - 1/2 \langle \operatorname{curl}(1/2 \operatorname{curl} u - \omega), u_h \rangle) dx. \end{aligned}$$

Thus, using that there holds for the exact solution $m = C_2(\nabla\omega)$, $\sigma = \mathcal{C}(\nabla u)$, and $\gamma = 2\mu_c(1/2 \operatorname{curl} u - \omega)$, we obtain together with the strong form (2.3) of Cosserat elasticity

$$\begin{aligned} & a((m, \sigma, \gamma), (m_h, \sigma_h, \gamma_h)) + b((m_h, \sigma_h, \gamma_h), (u, \omega)) + b((m, \sigma, \gamma), (u_h, \omega_h)) \\ &= \int_{\Omega} \left(\langle m, m_h \rangle_{C_2^{-1}} + \langle \sigma, \sigma_h \rangle_{\mathcal{C}^{-1}} + \frac{1}{2\mu_c} \langle \gamma, \gamma_h \rangle + \langle \operatorname{div} \sigma, u_h \rangle + \langle \operatorname{div} m, \omega_h \rangle - \langle \sigma_h, \nabla u \rangle \right. \\ & \quad \left. - \langle m_h, \nabla \omega \rangle - \langle 1/2 \operatorname{curl} u - \omega, \gamma_h \rangle + 2\mu_c \langle 1/2 \operatorname{curl} u - \omega, \omega_h \rangle - \mu_c \langle \operatorname{curl} (1/2 \operatorname{curl} u - \omega), u_h \rangle \right) dx \\ &= \int_{\Omega} (\langle \operatorname{div} \sigma, u_h \rangle + \langle \operatorname{div} m, \omega_h \rangle + 2\mu_c \langle 1/2 \operatorname{curl} u - \omega, \omega_h \rangle - \mu_c \langle \operatorname{curl} (1/2 \operatorname{curl} u - \omega), u_h \rangle) dx = -f(u_h, \omega_h). \end{aligned}$$

By subtracting the equations we directly obtain the Galerkin orthogonality (4.4). \square

4.2. Error analysis.

Definition 1 (Canonical interpolation operators). *We denote with $\mathcal{J}^{\operatorname{Ned}_{II},k} : C(\Omega, \mathbb{R}^3) \rightarrow \operatorname{Ned}_{II}^k$, $\mathcal{J}^{\operatorname{RT},k} : C(\Omega, \mathbb{R}^3) \rightarrow \operatorname{RT}^k$, $\mathcal{J}^{\operatorname{MCS},k} : C(\Omega, \mathbb{R}^{3 \times 3}) \rightarrow \operatorname{MCS}^k$, and $\mathcal{J}^{\operatorname{HHJ},k} : C(\Omega, \mathbb{R}_{\operatorname{sym}}^{3 \times 3}) \rightarrow \operatorname{HHJ}^k$ the canonical interpolation operators. $\mathcal{J}^{\operatorname{RT},k}$ is defined by the following equations on $T \in \mathcal{T}$ and $F \in \mathcal{F}$*

$$\int_F (\mathcal{J}^{\operatorname{RT},k} u - u)_n q \, ds = 0, \quad q \in \mathcal{P}^k(F), \quad \int_T \langle \mathcal{J}^{\operatorname{RT},k} u - u, q \rangle \, dx = 0, \quad q \in [\mathcal{P}^{k-1}(T)]^3.$$

For the definition of the other interpolation operators we refer to the literature, e.g., [23, 42, 37].

To extract convergence rates, we summarize the approximation properties of the canonical interpolation operators used in the analysis of the TDNNS and MCS methods.

Lemma 4. *Let $\mathcal{J}^{\operatorname{Ned}_{II},k}$, $\mathcal{J}^{\operatorname{RT},k}$, $\mathcal{J}^{\operatorname{MCS},k}$, and $\mathcal{J}^{\operatorname{HHJ},k}$ be the canonical interpolation operators from Definition 1, and $1 \leq l \leq k$. Assume that $u, \omega \in [H^1(\Omega)]^3 \cap [H^{l+1}(\mathcal{T})]^3$, $m \in \{\tau \in [H^{l+1}(\mathcal{T})]^{3 \times 3} : \llbracket \tau_{nt} \rrbracket = 0\}$, and $\sigma \in \{\tau \in [H^{l+1}(\mathcal{T})]_{\operatorname{sym}}^{3 \times 3} : \llbracket \tau_{nn} \rrbracket = 0\}$, where $H^{l+1}(\mathcal{T}) = \Pi_{T \in \mathcal{T}} H^{l+1}(T)$. Then there hold for a constant $C > 0$ independent of the mesh-size h the following estimates*

$$\begin{aligned} \|u - \mathcal{J}^{\operatorname{Ned}_{II},k} u\|_{V_h} &\leq Ch^l \|u\|_{H^{l+1}(\mathcal{T})}, & \|\omega - \mathcal{J}^{\operatorname{RT},k} \omega\|_{W_h} &\leq Ch^l \|\omega\|_{H^{l+1}(\mathcal{T})}, \\ \|\sigma - \mathcal{J}^{\operatorname{HHJ},k} \sigma\|_{L^2} + \sqrt{\sum_{F \in \mathcal{F}} h \|(\sigma - \mathcal{J}^{\operatorname{HHJ},k} \sigma)_{nn}\|_{L^2(F)}^2} &\leq Ch^{l+1} \|\sigma\|_{H^{l+1}(\mathcal{T})}, \\ \|m - \mathcal{J}^{\operatorname{MCS},k} m\|_{L^2} + \sqrt{\sum_{F \in \mathcal{F}} h \|(m - \mathcal{J}^{\operatorname{MCS},k} m)_{nt}\|_{L^2(F)}^2} &\leq Ch^{l+1} \|m\|_{H^{l+1}(\mathcal{T})}, \end{aligned}$$

where $\|\cdot\|_{V_h}$ and $\|\cdot\|_{W_h}$ are defined as in Theorem 1.

Proof. For the proof see [55, Theorem 4.21 and Theorem 4.23] and [24, Theorem 5.8, (6.13)] (noting the slightly different definition of the MCS space (3.10)). \square

Lemma 5. *There holds for $u \in [H^1(\Omega)]^3$ the following orthogonality property*

$$\langle \operatorname{div} \tau_h, u - \mathcal{J}^{\operatorname{RT},k} u \rangle_{H(\operatorname{div})^*} = 0, \quad \forall \tau_h \in \operatorname{MCS}^k.$$

Proof. Writing out the duality pairing (3.11) and noting that $\operatorname{div} \tau_h|_T \in [\mathcal{P}^{k-1}(T)]^3$ and $\tau_{h,nn} \in \mathcal{P}^k(F)$ the claim follows by the definition of the canonical RT interpolation operator from Definition 1

$$\langle \operatorname{div} \tau_h, u - \mathcal{J}^{\operatorname{RT},k} u \rangle_{H(\operatorname{div})^*} = \sum_{T \in \mathcal{T}} \int_T \langle \operatorname{div} \tau_h, u - \mathcal{J}^{\operatorname{RT},k} u \rangle \, dx - \sum_{F \in \mathcal{F}} \int_F \tau_{h,nn} (u - \mathcal{J}^{\operatorname{RT},k} u)_n \, ds = 0.$$

\square

Lemma 6. *Let $k \geq 1$ be an integer, $\sigma_h \in \text{HHJ}^k$, and $m_h \in \text{MCS}^k$. Then, there hold the following norm equivalencies, $a \simeq b$ if $a \leq Cb$ and $b \leq Ca$ for a constant $C > 0$ independent of the mesh-size,*

$$\|\sigma_h\|_{L^2}^2 \simeq \|\sigma_h\|_{L^2}^2 + h \sum_{F \in \mathcal{F}} \|\sigma_{h,nn}\|_{L^2(F)}^2, \quad \|m_h\|_{L^2}^2 \simeq \|m_h\|_{L^2}^2 + h \sum_{F \in \mathcal{F}} \|m_{h,nt}\|_{L^2(F)}^2.$$

Proof. Scaling arguments, see also [42, 23]. \square

Now, we are in the position to prove convergence, where the constant does not depend on μ_c .

Theorem 3 (Convergence). *Let (u, ω, m, σ) be the exact solution of linear Cosserat elasticity and $(u_h, \omega_h, m_h, \sigma_h, \gamma_h) \in \text{Ned}_{II}^k \times \text{RT}^{k-1} \times \text{MCS}^{k-1} \times \text{HHJ}^k \times \text{RT}^{k-1}$ the discrete solution of Problem 9. Assume for $0 \leq l \leq k-1$ the regularity $u \in [H^1(\Omega)]^3 \cap [H^{l+2}(\mathcal{T})]^3$, $\omega \in [H^1(\Omega)]^3 \cap [H^{l+1}(\mathcal{T})]^3$, $m \in [H^1(\Omega)]^{3 \times 3} \cap [H^{l+1}(\mathcal{T})]^{3 \times 3}$, and $\sigma \in [H^1(\Omega)]^{3 \times 3} \cap [H^{l+1}(\mathcal{T})]^{3 \times 3}$. Then there holds*

$$(4.5) \quad \begin{aligned} & \|u - u_h\|_{V_h} + \|\omega - \omega_h\|_{W_h} + \|m - m_h\|_{L^2} + \|\sigma - \sigma_h\|_{L^2} + \|\gamma - \gamma_h\|_{\Gamma} \\ & \leq Ch^l \left(\|u\|_{H^{l+1}} + \|\omega\|_{H^{l+1}} + \|m\|_{H^l} + \|\sigma\|_{H^l} + \frac{1}{\sqrt{\mu_c}} \|\gamma\|_{H^l} \right), \end{aligned}$$

$$(4.6) \quad \begin{aligned} & \|u - u_h\|_{V_h} + \|\omega_h - \mathcal{J}^{\text{RT}, k-1} \omega\|_{W_h} + \|m - m_h\|_{L^2} + \|\sigma - \sigma_h\|_{L^2} + \|\gamma - \gamma_h\|_{\Gamma} \\ & \leq Ch^{l+1} \left(\|u\|_{H^{l+2}} + \|m\|_{H^{l+1}} + \|\sigma\|_{H^{l+1}} + \frac{1}{\sqrt{\mu_c}} \|\gamma\|_{H^{l+1}} \right), \end{aligned}$$

where the norms $\|\cdot\|_{\Gamma}$, $\|\cdot\|_{V_h}$, $\|\cdot\|_{W_h}$ are defined as in Theorem 1 and $C \neq C(\mu_c)$.

Proof. Throughout the proof we use the notation $a \lesssim b$ if $a \leq Cb$ with a constant $C > 0$ independent of the mesh-size and μ_c . We add and subtract the canonical interpolation operators, apply the triangle inequality, and use the notation $\hat{u}_h := u_h - \mathcal{J}^{\text{Ned}_{II}, k} u$, $\hat{u} := u - \mathcal{J}^{\text{Ned}_{II}, k} u$, etc.,

$$\begin{aligned} & \|u - u_h\|_{V_h} + \|\omega - \omega_h\|_{W_h} + \|m - m_h\|_{L^2} + \|\sigma - \sigma_h\|_{L^2} + \|\gamma - \gamma_h\|_{\Gamma} \\ & \leq \|\hat{u}\|_{V_h} + \|\hat{\omega}\|_{W_h} + \|\hat{m}\|_{L^2} + \|\hat{\sigma}\|_{L^2} + \|\hat{\gamma}\|_{\Gamma} + \|\hat{u}_h\|_{V_h} + \|\hat{\omega}_h\|_{W_h} + \|\hat{m}_h\|_{L^2} + \|\hat{\sigma}_h\|_{L^2} + \|\hat{\gamma}_h\|_{\Gamma}. \end{aligned}$$

The first five terms can be estimated directly by the property of the interpolation operators Lemma 4

$$\|\hat{u}\|_{V_h} + \|\hat{\omega}\|_{W_h} + \|\hat{m}\|_{L^2} + \|\hat{\sigma}\|_{L^2} + \|\hat{\gamma}\|_{\Gamma} \lesssim h^l (\|u\|_{H^{l+1}} + \|\omega\|_{H^{l+1}} + \|m\|_{H^l} + \|\sigma\|_{H^l} + 1/\sqrt{\mu_c} \|\gamma\|_{H^l}).$$

For the remaining terms we use the inf-sup stability of Problem 9 and the Galerkin orthogonality (4.4) to obtain with $\|\cdot\|_{X_h}$, $\|\cdot\|_{Y_h}$ defined as in the proof of Theorem 1 and $Z_h := X_h \times Y_h$

$$\begin{aligned} & \|\hat{u}_h\|_{V_h} + \|\hat{\omega}_h\|_{W_h} + \|\hat{m}_h\|_{L^2} + \|\hat{\sigma}_h\|_{L^2} + \|\hat{\gamma}_h\|_{\Gamma} \leq \|(\hat{m}_h, \hat{\sigma}_h, \hat{\gamma}_h)\|_{X_h} + \|(\hat{u}_h, \hat{\omega}_h)\|_{Y_h} \\ & \lesssim \sup_{(\Psi_h, \Theta_h, \delta_h, v_h, \xi_h) \in Z_h} \frac{a((\hat{m}_h, \hat{\sigma}_h, \hat{\gamma}_h), (\Psi_h, \Theta_h, \delta_h)) + b((\hat{m}_h, \hat{\sigma}_h, \hat{\gamma}_h), (v_h, \xi_h)) + b((\Psi_h, \Theta_h, \delta_h), (\hat{u}_h, \hat{\omega}_h))}{\|(\Psi_h, \Theta_h, \delta_h)\|_{X_h} + \|(v_h, \xi_h)\|_{Y_h}} \\ & = \sup_{(\Psi_h, \Theta_h, \delta_h, v_h, \xi_h) \in Z_h} \frac{a((\hat{m}, \hat{\sigma}, \hat{\gamma}), (\Psi_h, \Theta_h, \delta_h)) + b((\hat{m}, \hat{\sigma}, \hat{\gamma}), (v_h, \xi_h)) + b((\Psi_h, \Theta_h, \delta_h), (\hat{u}, \hat{\omega}))}{\|(\Psi_h, \Theta_h, \delta_h)\|_{X_h} + \|(v_h, \xi_h)\|_{Y_h}}. \end{aligned}$$

Next, we estimate the bilinear forms a and b . For a we get with Cauchy-Schwarz inequality

$$|a((\hat{m}, \hat{\sigma}, \hat{\gamma}), (\Psi_h, \Theta_h, \delta_h))| \lesssim \|(\hat{m}, \hat{\sigma}, \hat{\gamma})\|_{X_h} \|(\Psi_h, \Theta_h, \delta_h)\|_{X_h}.$$

For the two expressions involving b we need to carefully treat the element boundary terms

$$\begin{aligned} |b((\hat{m}, \hat{\sigma}, \hat{\gamma}), (v_h, \xi_h))| & \leq \left| \sum_{T \in \mathcal{T}} - \int_T (\langle \hat{m}, \nabla \xi_h \rangle + \langle \hat{\sigma}, \nabla v_h \rangle) dx + \int_{\partial T} (\langle \hat{m}_{nt}, \xi_{h,t} \rangle + \hat{\sigma}_{nn} v_{h,n}) ds \right| \\ & \quad + \|\hat{\gamma}\|_{\Gamma} \sqrt{\mu_c} \|^{1/2} \text{curl } v_h - \xi_h\|_{L^2}. \end{aligned}$$

Noting that \hat{m} is tangential-normal continuous, we can estimate with Cauchy-Schwarz

$$\begin{aligned}
& \left| \sum_{T \in \mathcal{T}} \left(\int_T \langle \hat{m}, \nabla \xi_h \rangle dx - \int_{\partial T} \langle \hat{m}_{nt}, \xi_{h,t} \rangle ds \right) \right| \leq \left| \sum_{T \in \mathcal{T}} \int_T \langle \hat{m}, \nabla \xi_h \rangle dx \right| + \left| \sum_{F \in \mathcal{F}} \int_F \langle \hat{m}_{nt}, \llbracket \xi_{h,t} \rrbracket \rangle ds \right| \\
& \leq \sum_{T \in \mathcal{T}} \|\hat{m}\|_{L^2(T)} \|\nabla \xi_h\|_{L^2(T)} + \sum_{F \in \mathcal{F}} \sqrt{h} \|\hat{m}_{nt}\|_{L^2(F)} \frac{1}{\sqrt{h}} \|\llbracket \xi_{h,t} \rrbracket\|_{L^2(F)} \\
& \leq \|\hat{m}\|_{L^2} \sqrt{\sum_{T \in \mathcal{T}} \|\nabla \xi_h\|_{L^2(T)}^2} + \sqrt{\sum_{F \in \mathcal{F}} h \|\hat{m}_{nt}\|_{L^2(F)}^2} \sqrt{\sum_{F \in \mathcal{F}} \frac{1}{h} \|\llbracket \xi_{h,t} \rrbracket\|_{L^2(F)}^2} \\
& \lesssim \left(\|\hat{m}\|_{L^2} + \sqrt{\sum_{F \in \mathcal{F}} h \|\hat{m}_{nt}\|_{L^2(F)}^2} \right) \|\xi_h\|_{W_h}
\end{aligned}$$

and analogously as $\hat{\sigma}$ is normal-normal continuous and symmetric

$$\left| \sum_{T \in \mathcal{T}} \left(\int_T \langle \hat{\sigma}, \text{sym } \nabla v_h \rangle dx - \int_{\partial T} \hat{\sigma}_{nn} v_{h,n} ds \right) \right| \leq \left(\|\hat{\sigma}\|_{L^2} + \sqrt{\sum_{F \in \mathcal{F}} h \|\hat{\sigma}_{nn}\|_{L^2(F)}^2} \right) \|v_h\|_{V_h}.$$

Thus,

$$|b((\hat{m}, \hat{\sigma}, \hat{\gamma}), (v_h, \xi_h))| \lesssim \left(\|(\hat{m}, \hat{\sigma}, \hat{\gamma})\|_{X_h} + \sqrt{\sum_{F \in \mathcal{F}} h \|\hat{m}_{nt}\|_{L^2(F)}^2} + \sqrt{\sum_{F \in \mathcal{F}} h \|\hat{\sigma}_{nn}\|_{L^2(F)}^2} \right) \|(v_h, \xi_h)\|_{Y_h}.$$

For the second expression involving b we have

$$\begin{aligned}
b((\Psi_h, \Theta_h, \delta_h), (\hat{u}, \hat{\omega})) &= \sum_{T \in \mathcal{T}} \int_T (\langle \text{div } \Psi_h, \hat{\omega} \rangle - \langle \Theta_h, \nabla \hat{u} \rangle) dx - \int_{\partial T} (\Psi_{h,nn} \hat{\omega}_n - \Theta_{h,nn} \hat{u}_n) ds \\
&\quad - \int_{\Omega} \langle \delta_h, {}^{1/2} \text{curl } \hat{u} - \hat{\omega} \rangle dx.
\end{aligned}$$

Using Lemma 5 the terms involving Ψ_h are zero. The terms with Θ_h can be estimated in the same vein as before, using the equivalence of discrete norms in Lemma 6,

$$\left| \sum_{T \in \mathcal{T}} - \int_T \langle \Theta_h, \nabla \hat{u} \rangle dx + \int_{\partial T} \Theta_{h,nn} \hat{u}_n ds \right| \lesssim \|\Theta_h\|_{L^2} \|\hat{u}\|_{V_h}.$$

For the last term there holds with the commuting property of interpolants, $\text{curl } \mathcal{J}^{\text{Ned}^k_{II}} u = \mathcal{J}^{\text{RT}^{k-1}} \text{curl } u$,

$$\left| \int_{\Omega} \langle \delta_h, {}^{1/2} \text{curl } \hat{u} - \hat{\omega} \rangle dx \right| = \left| \int_{\Omega} \langle \delta_h, {}^{1/\mu_c} \hat{\gamma} \rangle dx \right| \leq \|\delta_h\|_{\Gamma} \|\hat{\gamma}\|_{\Gamma}.$$

Thus,

$$|b((\Psi_h, \Theta_h, \delta_h), (\hat{u}, \hat{\omega}))| \lesssim \|\Theta_h\|_{L^2} \|\hat{u}\|_{V_h} + \|\delta_h\|_{\Gamma} \|\hat{\gamma}\|_{\Gamma} \lesssim (\|\hat{u}\|_{V_h} + \|\hat{\gamma}\|_{\Gamma}) \|(\Theta_h, \Psi_h, \delta_h)\|_{X_h}.$$

Recognizing that the terms involving $\Psi_h, \Theta_h, \delta_h, v_h, \xi_h$ in the numerator and denominator of the supreme cancel, we obtain with Lemma 4 for $0 \leq l \leq k-1$

$$\begin{aligned}
& \|(\hat{m}_h, \hat{\sigma}_h, \hat{\gamma}_h)\|_{X_h} + \|(\hat{u}_h, \hat{\omega}_h)\|_{Y_h} \\
& \lesssim \|\hat{m}\|_{L^2} + \|\hat{\sigma}\|_{L^2} + \|\hat{\gamma}\|_{\Gamma} + \sqrt{\sum_{F \in \mathcal{F}} h \|\hat{m}_{nt}\|_{L^2(F)}^2} + \sqrt{\sum_{F \in \mathcal{F}} h \|\hat{\sigma}_{nn}\|_{L^2(F)}^2} + \|\hat{u}\|_{V_h} \\
(4.7) \quad & \lesssim h^l (\|m\|_{H^l} + \|\sigma\|_{H^l} + \|u\|_{H^{l+1}} + 1/\sqrt{\mu_c} \|\gamma\|_{H^l}),
\end{aligned}$$

which yields (4.5). For (4.6) we note that estimate (4.7) can be improved to h^{l+1} convergence as it is independent of ω_h . \square

Remark 3. For $k=1$ we do not obtain convergence for (4.5). The reason is that for the rotations ω_h the Raviart–Thomas space RT^0 does not contain the full linear polynomial space. Thanks to the orthogonality Lemma 5 the filtered error $\omega_h - \mathcal{J}_h^{\text{RT}^{k-1}}$ leads to super-convergence of the other fields.

Corollary 1 (Stability & convergence of Problem 6). *Adopt the assumptions from Theorem 3. Then, Problem 6 is stable, consistent and there hold the following error estimates*

$$\begin{aligned}
& \|u - u_h\|_{H^1} + \|\omega - \omega_h\|_{W_h} + \|m - m_h\|_{L^2} + \|\gamma - \gamma_h\|_{\Gamma} \\
& \leq Ch^l \left(\|u\|_{H^{l+1}} + \|\omega\|_{H^{l+1}} + \|m\|_{H^l} + \frac{1}{\sqrt{\mu_c}} \|\gamma\|_{H^l} \right), \\
& \|u - u_h\|_{H^1} + \|\omega_h - \mathcal{J}^{\text{RT}, k-1} \omega\|_{W_h} + \|m - m_h\|_{L^2} + \|\gamma - \gamma_h\|_{\Gamma} \\
& \leq Ch^{l+1} \left(\|u\|_{H^{l+2}} + \|m\|_{H^{l+1}} + \frac{1}{\sqrt{\mu_c}} \|\gamma\|_{H^{l+1}} \right).
\end{aligned}$$

Proof. Rewrite the elasticity part u in terms of an equivalent mixed method with $(u, \sigma) \in [H^1(\Omega)]^3 \times [L^2(\Omega)]_{\text{sym}}^{3 \times 3}$ and $(u_h, \sigma_h) \in \mathbf{Lag}^k \times [\mathcal{P}^{k-1}(\mathcal{T})]_{\text{sym}}^{3 \times 3}$. The proof of Theorems 1, 2, and 3 can readily be adapted by defining the norm $\|u_h\|_{V_h} = \|u_h\|_{H^1}$ and noting that $\langle \text{div } \sigma_h, u_h \rangle_{H(\text{curl})^*} = -\int_{\Omega} \langle \sigma_h, \nabla u_h \rangle dx$ simplifies to the L^2 integral. \square

4.3. Post-processing of rotations. From Theorem 3 and Corollary 1 we obtain that the rotation field ω_h converges with order $k-1$ in the W_h -norm, whereas the couple stress m_h converges with order k in the L^2 -norm. By the relation $\nabla \omega = C_2^{-1}(m)$, however, we can construct a rotation field $\tilde{\omega}_h$ with improved convergence rates. A standard approach is to solve the problem

$$\tilde{\omega}_h = \arg \min_{\substack{w_h \in [\mathcal{P}^k(\mathcal{T})]^3 \\ \int_T w_h dx = \int_T \omega_h dx, \forall T \in \mathcal{T}}} \|\nabla w_h - C_2^{-1}(m_h)\|_{L^2}.$$

It is well-known, see e.g. [56, 17], that $\tilde{\omega}_h$ converges in the L^2 -norm with one order more than m_h . However, we do not expect an improvement in the W_h -norm.

Motivated by [13], where a Nédélec function is post-processed such that improved convergence in a $H(\text{curl})$ -type norm is achieved, we propose a second type of post-processing. To this end, define e.g. $\text{BDM}^{k, \text{dc}}$ as the BDM space of order k , where the normal continuity is broken, i.e., the coupling degrees of freedom are doubled. Further, denote with $\text{RT}^{0, \text{dc}, *}$ the discrete elementwise dual space, whose degrees of freedom coincide with the canonical interpolant from Definition 1.

Problem 10 (Post-processing). *Let $(\omega_h, m_h) \in \text{RT}^{k-1} \times \text{MCS}^{k-1}$ be part of the solution of Problem 6 or Problem 8. Find $(\tilde{\omega}_h, \chi_h) \in \text{BDM}^{k,\text{dc}} \times \text{RT}^{0,\text{dc},*}$ such that for all $(\xi_h, \rho_h) \in \text{BDM}^{k,\text{dc}} \times \text{RT}^{0,\text{dc},*}$*

$$(4.8a) \quad \sum_{T \in \mathcal{T}} \int_T \langle \nabla \tilde{\omega}_h, \nabla \xi_h \rangle dx + \chi_h(\xi_h) = \sum_{T \in \mathcal{T}} \int_T \langle C_2^{-1}(m_h), \nabla \xi_h \rangle dx,$$

$$(4.8b) \quad \rho_h(\tilde{\omega}_h) = \rho_h(\omega_h).$$

Problem 10 can be solved elementwise. Equation (4.8b) states that $\mathcal{J}_h^{\text{RT}^0} \tilde{\omega}_h = \mathcal{J}_h^{\text{RT}^0} \omega_h$. Only the additional shape functions needed to go from RT^0 to BDM^k are optimized to fulfill the equation $\nabla \tilde{\omega}_h = C_2^{-1}(m_h)$ in an L^2 sense. For this post-processing, which we will use throughout, we observed also an increased convergence rate in the W_h -norm. A rigorous analysis of this post-processing scheme is, however, out of scope of this work and is topic of future research.

5. NUMERICAL EXAMPLES

All numerical examples are performed in the open-source finite element library NGSolve^a [51, 52].

method	description	reference
Lag ^k	Lagrangian elements for u and ω	Problem 2
M ^k	Lagrangian elements for u and MCS for ω	Problem 6
M-T ^k	TDNNS for u and MCS for ω	Problem 8

TABLE 1. Used Cosserat elasticity methods of polynomial order k for numerical examples.

The different methods for discretizing Cosserat elasticity are displayed in Table 1. For the couple stress problem we consider Problem 7 based on the MCS method.

We always compute the relative errors in the norms defined within Theorem 3 and Corollary 1, if not stated otherwise, and the respective estimated order of convergence (eoc). For comparison, the number of coupling degrees of freedom (ncdof) are considered. The displacement, rotation, elasticity stress, and couple stress errors read

$$u_{\text{err}} = \frac{\|u_h - u\|_{V_h}}{\|u\|_{H^1}}, \quad \omega_{\text{err}} = \frac{\|\omega_h - \omega\|_{W_h}}{\|\omega\|_{H^1}}, \quad \sigma_{\text{err}} = \frac{\|\sigma_h - \sigma\|_{L^2}}{\|\sigma\|_{L^2}}, \quad m_{\text{err}} = \frac{\|m_h - m\|_{L^2}}{\|m\|_{L^2}}.$$

When we use the MCS method to discretize the rotation field ω , we additionally compute the error of the post-processed $\tilde{\omega}_h$ from Problem 10.

The first three numerical benchmark examples will show that our methods perform well for basic bending and torsion responses. In Section 5.4 a challenging example to test for robustness in the Cosserat coupling constant μ_c is presented and in Section 5.5 we show the performance of our mixed formulation for the couple stress problem.

5.1. Cylindrical bending of plate. The first example we consider is a cylindrical bending of a thick plate [58] with length $L = 20$, height $H = 2$, and thickness $t = 20$, see Figure 1. The material parameters^b are chosen as $E = 2500$, $\nu \in \{0.25, 0.4999\}$ (and corresponding Lamé parameters $\mu = E/(2(1 + \nu))$, $\lambda = E\nu/((1 + \nu)(1 - 2\nu))$), $\mu_c = 0.5\mu$, $\alpha = 2\mu L_c^2$, $\beta = 2\mu L_c^2$, and $\gamma = 4\mu L_c^2$, with $L_c = 1$ the characteristic length. A bending moment $M_x = 100$ is applied on the left and right

^awww.ngsolve.org

^bIn [58] the authors use the parameters a, b, c , which are related by $\alpha = 4\mu c L_c^2$, $\beta = 4\mu b L_c^2$, $\gamma = 4\mu L_c^2$, $\mu_c = \mu a$.

boundary. To ensure a pure bending, couple stresses are given at the front and back boundary to compensate the effect of the Poisson ratio. The exact solution is given by

$$u_x = \frac{M_x xy}{D + \gamma H}, \quad u_y = -\frac{M_x}{2(D + \gamma H)} \left(x^2 + \frac{\nu}{1 - \nu} y^2 \right) + \frac{M_x}{24(D + \gamma H)} \left(L^2 + \frac{\nu}{1 - \nu} H^2 \right), \quad u_z = 0,$$

$$\omega_x = \omega_y = 0, \quad \omega_z = -\frac{M_x x}{D + \gamma H},$$

where $D = \frac{E H^3}{12(1 - \nu^2)}$. No body forces apply. The resulting non-zero stress components are

$$\sigma_{xx} = \frac{E}{1 - \nu^2} \frac{M_x y}{D + \gamma H}, \quad \sigma_{zz} = \frac{\nu E}{1 - \nu^2} \frac{M_x y}{D + \gamma H}, \quad m_{xz} = -\frac{\beta M_x}{D + \gamma H}, \quad m_{zx} = -\frac{\gamma M_x}{D + \gamma H}.$$

Due to symmetry only one quarter of the domain is meshed, and appropriate symmetry boundary conditions are prescribed. The other boundaries are left free, respectively, the bending forces are applied as Neumann boundary condition. To obtain a well-posed problem, the mean value of u_y is constraint to zero in terms of a Lagrange multiplier, noting that for the exact solution there holds $\int_{\Omega} u_y dx = 0$. We further note, that for quadratic elements the exact solution is exactly reproduced by all methods, showing consistency of the proposed methods. Thus, we consider in this benchmark only lowest-order linear elements for the displacements.

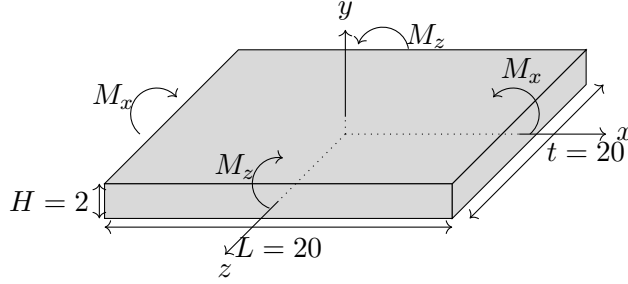


FIGURE 1. Geometry of cylindrical bending of a plate example.

To test for robustness in the nearly incompressible regime, Poisson ratios $\nu \in \{0.25, 0.4999\}$ are considered, where $\nu = 0.4999$ corresponds to an almost incompressible material. As displayed in Table 2 all proposed methods perform equally well for $\nu = 0.25$. Although the theory indicates only linear convergence for the fields (except for ω in the MCS settings), we observe higher convergence rates, which might come because of the low polynomial exact solution. For more complicated solutions this behavior vanishes. The MCS-TDNNS method is superior over the MCS method. This might be due to the plate structure with one dimension being smaller than the others and the TDNNS method is more robust with respect to anisotropic structures compared to a standard elasticity discretization by Lagrangian elements. In the nearly incompressible regime, $\nu = 0.4999$, we clearly observe reduced convergence for coarse meshes, cf. Table 3, except for the MCS-TDNNS method, highlighting the robustness of the TDNNS method for nearly incompressible elasticity. Especially, the stress σ_h can only be approximated well with the TDNNS method.

5.2. High-order bending. Next, we consider a high-order bending problem of a box with dimensions $L = H = t = 10$ [58], see Figure 2. The material parameters are the same as in Section 5.1.

The non-zero components of the exact solution are prescribed by

$$u_x = \frac{x \left(y - \frac{H}{2} \right)}{L}, \quad u_y = \tilde{u}_y - \frac{\int_{\Omega} \tilde{u}_y dx}{|\Omega|}, \quad \tilde{u}_y = -\frac{1.5}{L} x^2 - \frac{\lambda (2y - H)^2}{8L(\lambda + 2\mu)} + \frac{2x^3}{3L^2}, \quad \omega_z = -\frac{x^2}{L^2},$$

	ncdof	u_{err}	eoc	ω_{err}	eoc	$\tilde{\omega}_{\text{err}}$	eoc	σ_{err}	eoc	m_{err}	eoc
Lag ¹	139	0.4913	-	0.4519	-	-	-	1.0522	-	0.3960	-
	705	0.2549	0.95	0.2384	0.92	-	-	0.8688	0.28	0.2080	0.93
	4324	0.0861	1.56	0.0775	1.62	-	-	0.5306	0.71	0.0660	1.66
	29910	0.0262	1.72	0.0207	1.91	-	-	0.2801	0.92	0.0175	1.92
M ¹	432	0.4655	-	0.4812	-	0.4181	-	1.0543	-	0.3452	-
	2991	0.2385	0.96	0.3282	0.55	0.2208	0.92	0.8697	0.28	0.1916	0.85
	22296	0.0797	1.58	0.2672	0.30	0.0705	1.65	0.5281	0.72	0.0607	1.66
	172254	0.0246	1.70	0.2636	0.02	0.0187	1.92	0.2779	0.93	0.0160	1.92
M-T ¹	928	0.2240	-	0.3197	-	0.1910	-	0.7787	-	0.1684	-
	6543	0.1196	0.91	0.2800	0.19	0.1052	0.86	0.6093	0.35	0.0974	0.79
	49037	0.0470	1.35	0.2653	0.08	0.0366	1.52	0.3643	0.74	0.0328	1.57
	379481	0.0179	1.40	0.2643	0.01	0.0105	1.80	0.1958	0.90	0.0093	1.82

TABLE 2. Results of relative error of cylindrical bending of a plate with $\nu = 0.25$.

	ncdof	u_{err}	eoc	ω_{err}	eoc	$\tilde{\omega}_{\text{err}}$	eoc	σ_{err}	eoc	m_{err}	eoc
Lag ¹	139	0.6310	-	0.5821	-	-	-	12.2562	-	0.5288	-
	705	0.4979	0.34	0.4563	0.35	-	-	14.5771	-0.25	0.3943	0.42
	4324	0.2753	0.85	0.2547	0.84	-	-	17.8811	-0.29	0.2198	0.84
	29910	0.1080	1.35	0.0970	1.39	-	-	13.3613	0.42	0.0827	1.41
M ¹	432	0.6228	-	0.6084	-	0.5660	-	12.1592	-	0.4877	-
	2991	0.4938	0.34	0.4981	0.29	0.4511	0.33	14.5860	-0.26	0.3858	0.34
	22296	0.2729	0.86	0.3414	0.54	0.2522	0.84	17.8767	-0.29	0.2186	0.82
	172254	0.1071	1.35	0.2691	0.34	0.0961	1.39	13.3696	0.42	0.0826	1.40
M-T ¹	928	0.2416	-	0.3280	-	0.2062	-	0.5915	-	0.1821	-
	6543	0.1304	0.89	0.2827	0.21	0.1142	0.85	0.4517	0.39	0.1042	0.81
	49037	0.0509	1.36	0.2654	0.09	0.0395	1.53	0.2682	0.75	0.0351	1.57
	379481	0.0192	1.41	0.2643	0.01	0.0111	1.83	0.1428	0.91	0.0098	1.84

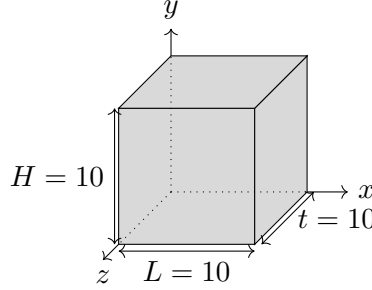
TABLE 3. Results of relative error of cylindrical bending of a plate with $\nu = 0.4999$.

FIGURE 2. Geometry of high-order bending of box example.

where u_y has zero mean. The resulting stresses and body forces can be computed by inserting the exact solution into the strong form of Cosserat elasticity (2.3). For the boundary conditions we fix u_x at $x = 0$ and u_z at $z = 0$ and $z = t$. Further, $\omega_x = 0$ at $z = 0$ and $z = t$, $\omega_y = 0$ at $x = 0$, $z = 0$, and $z = t$, as well as $\omega_z = 0$ at $x = 0$. The zero mean of u_y is enforced by a Lagrange multiplier.

In Table 4 and Table 5 we display the convergence rates for linear and quadratic elements, respectively. We note, that cubic ansatz functions would resemble the exact solution. Again, due to the simple form of the exact solution, parts of the fields converge super-optimal. However, all three methods show the same convergence behavior.

5.3. Torsion of a cylinder. A cylinder with length $L = 1$ and radius $R = 0.2$ is exposed to a torsion force T at the top and bottom anti-symmetrically, see Figure 3. We consider the material

	ncdof	u_{err}	eoc	ω_{err}	eoc	$\tilde{\omega}_{\text{err}}$	eoc	σ_{err}	eoc	m_{err}	eoc
Lag ¹	23	0.4974	-	0.7595	-	-	-	0.7053	-	0.8540	-
	136	0.2567	0.95	0.3625	1.07	-	-	0.4649	0.60	0.3519	1.28
	920	0.0910	1.50	0.1226	1.56	-	-	0.2574	0.85	0.1395	1.34
	6736	0.0312	1.55	0.0354	1.79	-	-	0.1328	0.95	0.0596	1.23
M ¹	94	0.5185	-	0.9089	-	0.6098	-	0.7068	-	0.6001	-
	679	0.2493	1.06	0.5261	0.79	0.3003	1.02	0.4657	0.60	0.3407	0.82
	5197	0.0871	1.52	0.3934	0.42	0.1071	1.49	0.2578	0.85	0.1576	1.11
	40729	0.0303	1.52	0.3774	0.06	0.0344	1.64	0.1332	0.95	0.0720	1.13
M-T ¹	203	0.3082	-	0.6615	-	0.3262	-	0.4655	-	0.4890	-
	1485	0.1628	0.92	0.4540	0.54	0.1773	0.88	0.3292	0.50	0.2838	0.79
	11417	0.0634	1.36	0.3860	0.23	0.0699	1.34	0.1854	0.83	0.1416	1.00
	89649	0.0253	1.33	0.3776	0.03	0.0265	1.40	0.0970	0.93	0.0692	1.03

TABLE 4. Results of relative error for high-order bending of box for $k = 1$.

	ncdof	u_{err}	eoc	ω_{err}	eoc	$\tilde{\omega}_{\text{err}}$	eoc	σ_{err}	eoc	m_{err}	eoc
Lag ²	136	0.0606	-	0.0448	-	-	-	0.1800	-	0.0808	-
	920	0.0096	2.66	0.0047	3.25	-	-	0.0442	2.03	0.0143	2.50
	6736	0.0021	2.16	0.0006	3.05	-	-	0.0114	1.96	0.0021	2.76
	51488	0.0005	2.04	0.0001	3.02	-	-	0.0029	1.98	0.0003	2.92
M ²	313	0.0582	-	0.1493	-	0.0320	-	0.1862	-	0.0967	-
	2293	0.0096	2.61	0.0594	1.33	0.0039	3.04	0.0458	2.02	0.0166	2.54
	17593	0.0022	2.15	0.0286	1.05	0.0005	2.92	0.0118	1.96	0.0024	2.77
	137905	0.0005	2.04	0.0143	1.00	0.0001	2.97	0.0030	1.98	0.0003	2.92
M-T ²	547	0.0427	-	0.1422	-	0.0192	-	0.1285	-	0.0770	-
	4063	0.0084	2.35	0.0589	1.27	0.0031	2.64	0.0333	1.95	0.0144	2.42
	31381	0.0020	2.09	0.0286	1.04	0.0004	2.91	0.0087	1.94	0.0021	2.77
	246793	0.0005	2.03	0.0143	1.00	0.0001	2.95	0.0022	1.97	0.0003	2.92

TABLE 5. Results of relative error for high-order bending of box for $k = 2$.

parameters^c $\mu = 15$, $\lambda = 1$, $\mu_c = 5$, and $\alpha = \beta = \gamma = 0.5$. The exact solution derived in [21] reads in cylindrical coordinates (r, θ, z) , with $r = \sqrt{x^2 + y^2}$, $\theta = \arctan(y, x)$,

$$u_r = u_z = 0, \quad u_\theta = C_1 r z, \quad \omega_r = -\frac{C_1 r}{2} + C_2 I_1(p r), \quad \omega_z = C_1 z, \quad \omega_\theta = 0,$$

$$e_r = (x^2 + y^2)^{-1/2} \begin{pmatrix} x & y & 0 \end{pmatrix}^T, \quad e_\theta = (x^2 + y^2)^{-1/2} \begin{pmatrix} -y & x & 0 \end{pmatrix}^T, \quad e_z = \begin{pmatrix} 0 & 0 & 1 \end{pmatrix}^T,$$

where $I_n(\cdot)$ is the modified Bessel function of first kind of order n and

$$C_1 = 2C_2 \left(\frac{\alpha + \beta + \gamma}{\beta + \gamma} p I_0(p R) - \frac{I_1(p R)}{R} \right), \quad p = \sqrt{\frac{4\mu_c}{\alpha + \beta + \gamma}},$$

$$C_2 = \frac{T}{2\pi R^2} \left(\left(\frac{2\mu}{\beta + \gamma} \frac{R^2}{4} + \frac{3}{2} \right) (\alpha + \beta + \gamma) p I_0(p R) - \left(\frac{2\mu}{\beta + \gamma} \frac{R^2}{4} + 2 \right) (\beta + \gamma) \frac{I_1(p a R)}{R} \right)^{-1}.$$

By symmetry in z -direction we consider half of the domain. All other boundaries are free except the top, where the torsion is applied. We enforce zero mean-value for the x and y displacement and rotation quantities by Lagrange multipliers (the exact solution also has zero mean). Note, that the resulting couple stress m is symmetric independently of the choice of β and γ for this benchmark as only m_{rr} , $m_{\theta\theta}$, and m_{zz} are non-zero [21]. We use linear, quadratic, and cubic elements.

To reduce the geometry approximation error due to the curved cylindrical domain, we curve the boundary with polynomial degree $k - 1$. An isoperimetric approach would be to curve the boundary equally with the displacement and rotation order k for the Lagrangian method Lag^k. However, we

^cIn [21] the parameters $\tilde{\mu}$ and κ are used, which are related by $\mu = \tilde{\mu} + \kappa/2$, $\mu_c = 2\kappa$.

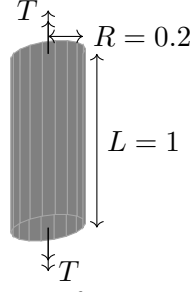
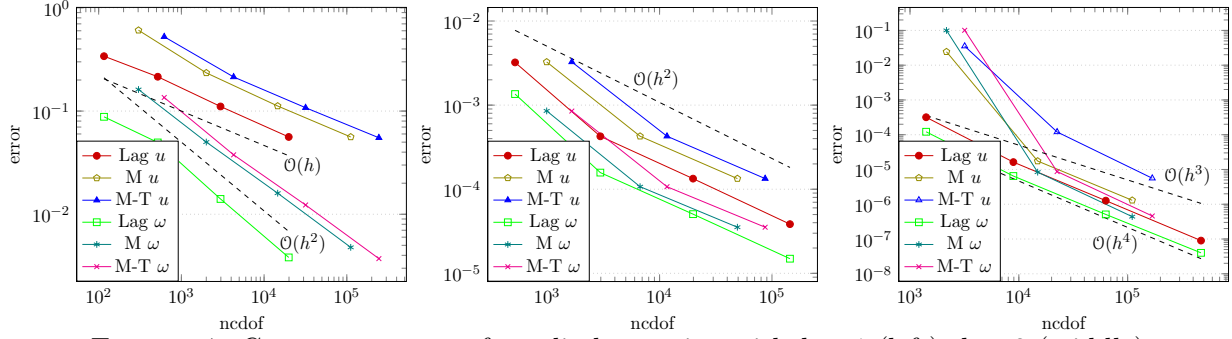


FIGURE 3. Geometry of torsion of cylinder example.

FIGURE 4. Convergence rates for cylinder torsion with $k = 1$ (left), $k = 2$ (middle), and $k = 3$ (right). For M^k and $M-T^k$ $\tilde{\omega}_h$ is used instead of ω_h .

use RT^{k-1} for the rotation field in the MCS methods, which does not contain all polynomials of degree k . Thus, curving would reduce the accuracy of the method instead of increasing because the polynomials do not get preserved during the mapping. We observe a comparable convergence behavior for all three methods, see Figure 4. The pure MCS method is superior by a constant compared to the MCS-TDNNs method, however, the same overall convergence rates are obtained. Due to the strong symmetries of the solution, some super-convergence can be observed.

5.4. Convergence and robustness in the Cosserat coupling constant. So far the Cosserat coupling constant μ_c was well-behaved in the previous numerical examples. To test robustness in the Cosserat coupling constant $\mu_c \rightarrow \infty$ we adapt the example from Section 5.2. We consider the domain $\Omega = (0, 1)^3$ and the material parameters $E = 2500$, $\nu = 0.25$ (and corresponding Lamé parameters μ and λ), $L_c = 1$, $\alpha = \beta = 2\mu L_c^2$, and $\gamma = 4\mu L_c^2$. Then we consider a sequence of Cosserat coupling moduli $\mu_c \in \{\mu, \mu \times 10^3, \mu \times 10^6\}$. We assume that the exact solution is given by

$$u_x = \sin(x)(y - 1/2), \quad u_y = -1/2 \sin(x)^2 - \sin(x)^2 \frac{\lambda}{2(\lambda + 2\mu)} (y - 1/2)^2 \cos(z) + \frac{\sin(x)^3}{3},$$

$$u_z = \sin(x)^2 \cos(1 - y)(z - 1/2), \quad \omega = 1/2 \operatorname{curl} u + \frac{1}{\mu_c} \nabla \Phi, \quad \Phi = 10^3 x^2 (1 - x) y (1 - y) (1 - z)^2$$

and the corresponding right-hand sides can be computed by inserting the exact solution into the strong form (2.3). At the boundary $x = 0$ we have homogeneous Dirichlet data for u and ω (clamped boundary), the other boundaries are of Neumann type. Note, that in the limit $\mu_c \rightarrow \infty$ there holds for the exact solution $\omega = 1/2 \operatorname{curl} u$, i.e., the couple stress problem is obtained.

In Table 6, Table 7, and Table 8 the results for the linear methods are displayed. We observe for the case $\mu_c = \mu$ in Table 6 that all three methods perform equally well. No locking is observed. Increasing the Cosserat coupling constant to $\mu_c = \mu \times 10^3$, however, yields an increased so-called

	ncdof	u_{err}	eoc	ω_{err}	eoc	$\tilde{\omega}_{\text{err}}$	eoc	σ_{err}	eoc	m_{err}	eoc
Lag ^I	30	0.6248	-	0.6333	-	-	-	0.5892	-	0.7437	-
	156	0.3494	0.84	0.3337	0.92	-	-	0.3642	0.69	0.4115	0.85
	984	0.1846	0.92	0.1823	0.87	-	-	0.1921	0.92	0.2269	0.86
	6960	0.0936	0.98	0.0943	0.95	-	-	0.0975	0.98	0.1169	0.96
	52320	0.0470	0.99	0.0478	0.98	-	-	0.0489	1.00	0.0590	0.99
M ^I	99	0.5843	-	1.2808	-	0.8426	-	0.6296	-	0.7276	-
	702	0.3444	0.76	1.2522	0.03	0.4509	0.90	0.3667	0.78	0.3913	0.89
	5292	0.1840	0.90	1.2940	-0.05	0.2442	0.88	0.1929	0.93	0.2107	0.89
	41112	0.0936	0.98	1.3186	-0.03	0.1221	1.00	0.0978	0.98	0.1063	0.99
	324144	0.0470	0.99	1.3326	-0.02	0.0608	1.00	0.0491	1.00	0.0533	1.00
M-T ^I	210	0.5654	-	1.3104	-	0.8669	-	0.3566	-	0.7402	-
	1524	0.3125	0.86	1.2584	0.06	0.4533	0.94	0.1925	0.89	0.3927	0.91
	11592	0.1696	0.88	1.2957	-0.04	0.2445	0.89	0.1065	0.85	0.2108	0.90
	90384	0.0873	0.96	1.3191	-0.03	0.1221	1.00	0.0554	0.94	0.1063	0.99
	713760	0.0442	0.98	1.3327	-0.01	0.0608	1.01	0.0282	0.98	0.0533	1.00

TABLE 6. Results robustness for Cosserat coupling constant $\mu_c = \mu$.

	ncdof	u_{err}	eoc	ω_{err}	eoc	$\tilde{\omega}_{\text{err}}$	eoc	σ_{err}	eoc	m_{err}	eoc
Lag ^I	30	0.9805	-	0.9650	-	-	-	0.9333	-	0.9643	-
	156	0.7422	0.40	0.8471	0.19	-	-	0.5656	0.72	0.8422	0.20
	984	0.4997	0.57	0.5768	0.55	-	-	0.4081	0.47	0.5625	0.58
	6960	0.2331	1.10	0.2565	1.17	-	-	0.2235	0.87	0.2452	1.20
	52320	0.0910	1.36	0.0835	1.62	-	-	0.1120	1.00	0.0818	1.58
M ^I	99	0.7587	-	1.1637	-	0.5918	-	0.8166	-	0.5447	-
	702	0.4261	0.83	1.1997	-0.04	0.3082	0.94	0.5419	0.59	0.2934	0.89
	5292	0.2407	0.82	1.2878	-0.10	0.1539	1.00	0.3467	0.64	0.1480	0.99
	41112	0.1260	0.93	1.3208	-0.04	0.0770	1.00	0.1897	0.87	0.0737	1.01
	324144	0.0642	0.97	1.3352	-0.02	0.0406	0.92	0.0978	0.96	0.0381	0.95
M-T ^I	210	0.6232	-	1.1915	-	0.6402	-	0.4062	-	0.5663	-
	1524	0.3308	0.91	1.2223	-0.04	0.3275	0.97	0.2174	0.90	0.2864	0.98
	11592	0.1790	0.89	1.2929	-0.08	0.1664	0.98	0.1195	0.86	0.1483	0.95
	90384	0.0922	0.96	1.3213	-0.03	0.0844	0.98	0.0622	0.94	0.0763	0.96
	713760	0.0467	0.98	1.3350	-0.01	0.0426	0.99	0.0317	0.97	0.0389	0.97

TABLE 7. Results robustness for Cosserat coupling constant $\mu_c = \mu \times 10^3$.

	ncdof	u_{err}	eoc	ω_{err}	eoc	$\tilde{\omega}_{\text{err}}$	eoc	σ_{err}	eoc	m_{err}	eoc
Lag ^I	30	1.0071	-	1.0000	-	-	-	0.9554	-	1.0000	-
	156	0.8425	0.26	0.9998	0.00	-	-	0.5816	0.72	0.9998	0.00
	984	0.8061	0.06	0.9992	0.00	-	-	0.4954	0.23	0.9991	0.00
	6960	0.7854	0.04	0.9968	0.00	-	-	0.4070	0.28	0.9965	0.00
	52320	0.7725	0.02	0.9873	0.01	-	-	0.3673	0.15	0.9862	0.01
M ^I	99	0.7612	-	1.1649	-	0.5931	-	0.8193	-	0.5458	-
	702	0.4285	0.83	1.2006	-0.04	0.3104	0.93	0.5456	0.59	0.2968	0.88
	5292	0.2432	0.82	1.2878	-0.10	0.1581	0.97	0.3507	0.64	0.1531	0.95
	41112	0.1289	0.92	1.3206	-0.04	0.0817	0.95	0.1932	0.86	0.0796	0.94
	324144	0.0692	0.90	1.3354	-0.02	0.0450	0.86	0.1022	0.92	0.0434	0.87
M-T ^I	210	0.6224	-	1.1899	-	0.6388	-	0.4058	-	0.5663	-
	1524	0.3307	0.91	1.2208	-0.04	0.3253	0.97	0.2174	0.90	0.2851	0.99
	11592	0.1789	0.89	1.2919	-0.08	0.1626	1.00	0.1196	0.86	0.1455	0.97
	90384	0.0922	0.96	1.3209	-0.03	0.0806	1.01	0.0622	0.94	0.0728	1.00
	713760	0.0467	0.98	1.3349	-0.02	0.0400	1.01	0.0317	0.97	0.0363	1.00

TABLE 8. Results robustness for Cosserat coupling constant $\mu_c = \mu \times 10^6$.

pre-asymptotic regime for the pure Lagrangian method Lag¹. This pre-asymptotic regime can also be clearly observed in Figure 5 (left), where the mesh resolution has to be sufficiently fine before the optimal convergence rate starts. The two mixed methods do not show this locking phenomenon as expected by the convergence Theorem 3 and Corollary 1, where the constant C has been proved to be independent of the Cosserat coupling constant μ_c , cf. Table 7. Even by increasing the constant to $\mu_c = \mu \times 10^6$, which already almost resembles the coupled stress limit problem, the mixed methods converge optimally. In contrast, the Lagrangian based method Lag¹ nearly stops converging, the pre-asymptotic regime completely dominates, see Table 8 and Figure 5 (left). Increasing the polynomial ansatz space from linear to quadratic elements reduces the enormous locking problem for Lag². Nevertheless, one can observe in Figure 5 (right) that the convergence is not independent of μ_c , the curves shift strongly. The convergence for the quadratic mixed methods, however, show the same behavior as their linear counter-parts.

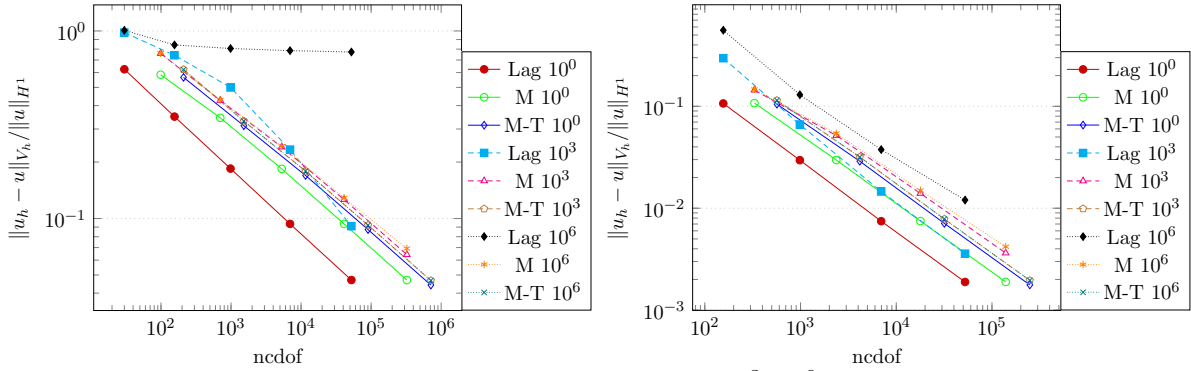


FIGURE 5. Results robustness test for $\mu_c/\mu \in \{1, 10^3, 10^6\}$ with methods of order $k = 1$ (left) and $k = 2$ (right).

5.5. Shearing of plate with couple stress problem. For demonstrating our mixed formulation Problem 7 for the couple stress problem (2.12) we consider the following shearing problem proposed in [41], see Figure 6 (left) for the geometry of a box with dimensions $H = 30$, $L = t = 150$. On the bottom the plate is clamped and on the top the y and z components are fixed and an x -displacement of $\bar{u} = 1$ is given. Symmetry boundary conditions at $z = 0$ are prescribed. We consider the material parameters $E = 2500$, $\nu = 0.25$, $\beta = \gamma = 0.5\mu L_c^2$, and a sequence of characteristic lengths $L_c = 2, 8, 32$. Note that the Cosserat coupling constant μ_c (was set formally to ∞) and α (is undetermined, cf. (2.14)) do not appear. The exact solution reads^d

$$u_x = c_1 + c_2 y + c_3 e^{\frac{2y}{L_c}} + c_4 e^{-\frac{2y}{L_c}}, \quad u_y = u_z = 0, \quad \Psi = \bar{u} \left(L_c \left(1 - e^{\frac{2h}{L_c}} \right) + h \left(1 + e^{\frac{2h}{L_c}} \right) \right)^{-1}, \quad \chi = \frac{L_c}{2} \Psi,$$

$$c_1 = \chi \left(1 - e^{\frac{2h}{L_c}} \right), \quad c_2 = \Psi \left(1 + e^{\frac{2h}{L_c}} \right), \quad c_3 = -\chi, \quad c_4 = e^{\frac{2h}{L_c}} \chi.$$

Note, that in the limit $L_c = 0$ of classical elasticity the exact solution reads $u_x = \bar{u}y/H$. The corresponding stresses and body forces can be computed by inserting the exact solution into the strong form of the couple stress problem (2.13).

In Figure 6 (right) the exact solution for characteristic lengths $L_c = 0, 2, 8, 32, 128$ are displayed along the line $x = z = 0$. Therein the change of behavior of the solution with respect to L_c can be observed. Due to the smoothness of the exact solution and the change of displacement close to the top and bottom boundary, we expect that polynomial refinement will lead to accurate

^dThe constants c_1, c_2, c_3, c_4 (49a-d) in [41] have been corrected here to fulfill the equations (46a-d).

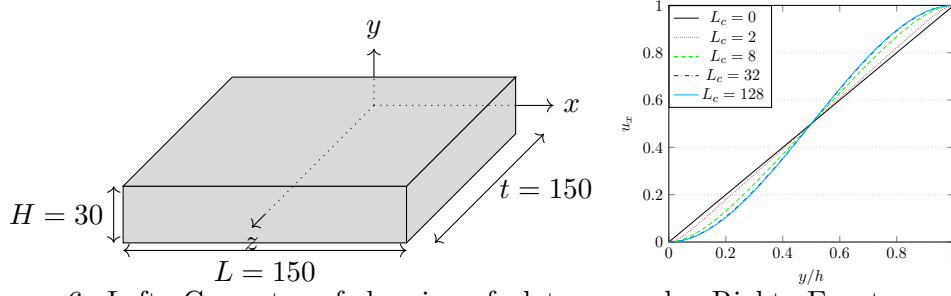


FIGURE 6. Left: Geometry of shearing of plate example. Right: Exact u_x at line $x = z = 0$ for $L_c \in \{0, 2, 8, 32, 128\}$ (the curves for $L_c = 32, 128$ nearly overlap).

approximations. To this end, we fix an initial mesh consisting of 528 unstructured tetrahedra and solve the couple stress problem with polynomial orders $k = 1, 2, 3, 4$. In Figure 7 we see that the low-order method $k = 1$ completely fails to capture the solution's behavior on the coarse mesh for all characteristic lengths. For $L_c = 2$ also the quadratic method suffers accuracy, but yields better solutions for $L_c = 8$ and $L_c = 32$. Using cubic and quartic polynomial orders the exact solutions get approximated well for all characteristic lengths. Only for $L_c = 2$ the curves are not overlapping.

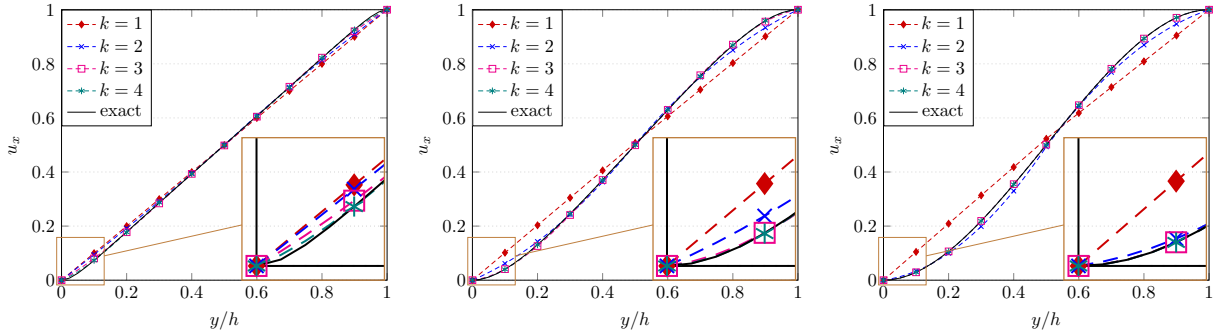


FIGURE 7. u_x at line $x = z = 0$. Left: $L_c = 2$. Middle: $L_c = 8$. Right: $L_c = 32$.

ACKNOWLEDGMENTS

The work of Kaibo Hu was supported by a Royal Society University Research Fellowship (URF\R1\221398). Michael Neunteufel acknowledges support by the National Science Foundation (USA).

REFERENCES

- [1] H. ALTENBACH AND V. A. EREMEYEV, eds., *Generalized Continua from the Theory to Engineering Applications*, vol. 541 of CISM Courses and Lectures, Springer, 2010.
- [2] D. N. ARNOLD, *Finite element exterior calculus*, SIAM, 2018.
- [3] D. N. ARNOLD, R. S. FALK, AND R. WINTHER, *Finite element exterior calculus, homological techniques, and applications*, Acta numerica, 15 (2006), pp. 1–155.
- [4] ———, *Finite element exterior calculus: from Hodge theory to numerical stability*, Bulletin of the American Mathematical Society, 47 (2010), pp. 281–354.
- [5] D. N. ARNOLD AND K. HU, *Complexes from complexes*, Foundations of Computational Mathematics, (2021), pp. 1–36.
- [6] D. BOFFI, F. BREZZI, AND M. FORTIN, *Mixed Finite Element Methods and Applications*, Springer, 2013.
- [7] W. M. BOON, O. DURAN, AND J. M. NORDBOTTEN, *Mixed finite element methods for linear cosserat equations*, 2024.
- [8] D. BRAESS AND J. SCHÖBERL, *Equilibrated residual error estimator for edge elements*, Mathematics of Computation, 77 (2008), pp. 651–672.

- [9] F. BREZZI, *On the existence, uniqueness and approximation of saddle-point problems arising from Lagrangian multipliers*, Revue française d'automatique, informatique, recherche opérationnelle. Analyse numérique, 8 (1974), pp. 129–151.
- [10] F. BREZZI, J. DOUGLAS JR, AND L. D. MARINI, *Two families of mixed finite elements for second order elliptic problems*, Numerische Mathematik, 47 (1985), pp. 217–235.
- [11] A. ČAP AND K. HU, *BGG sequences with weak regularity and applications*, Foundations of Computational Mathematics, (2023), pp. 1–40.
- [12] S. CHAKRAVARTY, A. R. HADJESFANDIARI, AND G. F. DARGUSH, *A penalty-based finite element framework for couple stress elasticity*, Finite Elements in Analysis and Design, 130 (2017), pp. 65–79.
- [13] L. CHEN, X. HUANG, AND C. ZHANG, *Distributional Finite Element curl div Complexes and Application to Quad Curl Problems*, 2023.
- [14] J.-H. CHOI, B.-C. LEE, AND G.-D. SIM, *A 10-node tetrahedral element with condensed Lagrange multipliers for the modified couple stress theory*, Computers & Structures, 246 (2021), p. 106476.
- [15] S. H. CHRISTIANSEN, *On the linearization of Regge calculus*, Numerische Mathematik, 119 (2011), pp. 613–640.
- [16] S. H. CHRISTIANSEN, K. HU, AND T. LIN, *Extended Regge complex for linearized Riemann-Cartan geometry and cohomology*, arXiv preprint arXiv:2312.11709, (2023).
- [17] B. COCKBURN, J. GOPALAKRISHNAN, AND F.-J. SAYAS, *A projection-based error analysis of HDG methods*, Mathematics of Computation, 79 (2010), pp. 1351–1367.
- [18] E. COSSERAT AND F. COSSERAT, *Théories des Corps Déformables*, Hermann, Paris, 1909.
- [19] L. B. DA VEIGA, J. NIIRANEN, AND R. STENBERG, *A Family of C^0 Finite Elements For Kirchhoff Plates I: Error Analysis*, SIAM Journal on Numerical Analysis, 45 (2007), pp. 2047–2071.
- [20] N. GARG AND C.-S. HAN, *A penalty finite element approach for couple stress elasticity*, Computational Mechanics, 52 (2013), pp. 709–720.
- [21] R. D. GAUTHIER AND W. E. JAHSMAN, *A Quest for Micropolar Elastic Constants*, Journal of Applied Mechanics, 42 (1975), pp. 369–374.
- [22] J. GOPALAKRISHNAN, L. KOGLER, P. L. LEDERER, AND J. SCHÖBERL, *Divergence-Conforming Velocity and Vorticity Approximations for Incompressible Fluids Obtained with Minimal Facet Coupling*, Journal of Scientific Computing, 95 (2023), p. 91.
- [23] J. GOPALAKRISHNAN, P. L. LEDERER, AND J. SCHÖBERL, *A mass conserving mixed stress formulation for Stokes flow with weakly imposed stress symmetry*, SIAM Journal on Numerical Analysis, 58 (2020), pp. 706–732.
- [24] J. GOPALAKRISHNAN, P. L. LEDERER, AND J. SCHÖBERL, *A mass conserving mixed stress formulation for the Stokes equations*, IMA Journal of Numerical Analysis, 40 (2020), pp. 1838–1874.
- [25] S. GRBČIĆ, A. IBRAHIMBEGOVIĆ, AND G. JELENIĆ, *Variational formulation of micropolar elasticity using 3D hexahedral finite-element interpolation with incompatible modes*, Computers & Structures, 205 (2018), pp. 1–14.
- [26] W. GÜNTHER, *Zur Statik und Kinematik des Cosseratschen Kontinuums*, Abhandlungen der Braunschweigischen Wissenschaftlichen Gesellschaft, (1958).
- [27] K. HELLAN, *Analysis of elastic plates in flexure by a simplified finite element method*, Acta Polytechnica Scandinavica, Civil Engineering Series, 46 (1967).
- [28] L. R. HERRMANN, *Finite element bending analysis for plates*, Journal of the Engineering Mechanics Division, 93 (1967), pp. 13–26.
- [29] K. HU, T. LIN, AND Q. ZHANG, *Distributional Hessian and divdiv complexes on triangulation and cohomology*, arXiv preprint arXiv:2311.15482, (2023).
- [30] J. JEONG AND P. NEFF, *Existence, Uniqueness and Stability in Linear Cosserat Elasticity for Weakest Curvature Conditions*, Mathematics and Mechanics of Solids, 15 (2010), pp. 78–95.
- [31] C. JOHNSON, *On the convergence of a mixed finite element method for plate bending moments*, Numerische Mathematik, 21 (1973), pp. 43–62.
- [32] R. S. LAKES, *Experimental evaluation of micromorphic elastic constants in foams and lattices*, Zeitschrift für angewandte Mathematik und Physik (ZAMP), 74 (2023).
- [33] G. MAUGIN AND A. METRIKINE, eds., *Mechanics of Generalized Continua – One Hundred Years After the Cosserats*, vol. 21 of Advances in Mechanics and Mathematics, Springer, 2010.
- [34] J. NÉDÉLEC, *A new family of mixed finite elements in \mathbb{R}^3* , Numerische Mathematik, 50 (1986), pp. 57–81.
- [35] P. NEFF AND J. JEONG, *A new paradigm: The linear isotropic Cosserat model with conformally invariant curvature energy*, Journal of Applied Mathematics and Mechanics/Zeitschrift für Angewandte Mathematik und Mechanik (ZAMM), 89 (2009), p. 107.

- [36] P. NEFF, J. JEONG, AND A. FISCHLE, *Stable identification of linear isotropic Cosserat parameters: Bounded stiffness in bending and torsion implies conformal invariance of curvature*, Acta Mechanica, 211 (2010), pp. 237–249.
- [37] M. NEUNTEUFEL, *Mixed Finite Element Methods for Nonlinear Continuum Mechanics and Shells*, PhD thesis, TU Wien, 2021.
- [38] M. NEUNTEUFEL, A. S. PECHSTEIN, AND J. SCHÖBERL, *Three-field mixed finite element methods for nonlinear elasticity*, Computer Methods in Applied Mechanics and Engineering, 382 (2021), p. 113857.
- [39] M. NEUNTEUFEL AND J. SCHÖBERL, *The Hellan–Herrmann–Johnson method for nonlinear shells*, Computers & Structures, 225 (2019), p. 106109.
- [40] ———, *The Hellan–Herrmann–Johnson and TDNNS methods for linear and nonlinear shells*, Computers & Structures, 305 (2024), p. 107543.
- [41] S. K. PARK AND X.-L. GAO, *Variational formulation of a modified couple stress theory and its application to a simple shear problem*, Zeitschrift für angewandte Mathematik und Physik, 59 (2008), pp. 904–917.
- [42] A. PECHSTEIN AND J. SCHÖBERL, *Tangential-displacement and normal-normal-stress continuous mixed finite elements for elasticity*, Mathematical Models and Methods in Applied Sciences, 21 (2011), pp. 1761–1782.
- [43] A. PECHSTEIN AND J. SCHÖBERL, *Anisotropic mixed finite elements for elasticity*, International Journal for Numerical Methods in Engineering, 90 (2012), pp. 196–217.
- [44] A. PECHSTEIN AND J. SCHÖBERL, *The TDNNS method for Reissner–Mindlin plates*, Numerische Mathematik, 137 (2017), pp. 713–740.
- [45] E. PROVIDAS AND M. KATTIS, *Finite element method in plane Cosserat elasticity*, Computers & Structures, 80 (2002), pp. 2059–2069.
- [46] P. RAVIART AND J. THOMAS, *A mixed finite element method for second order elliptic problems*, Lecture Notes in Mathematics, 606 (1977), pp. 292–315.
- [47] T. REGGE, *General relativity without coordinates*, Il Nuovo Cimento (1955-1965), 19 (1961), pp. 558–571.
- [48] A. RIAHI AND J. H. CURRAN, *Full 3D finite element Cosserat formulation with application in layered structures*, Applied mathematical modelling, 33 (2009), pp. 3450–3464.
- [49] Z. RUEGER AND R. S. LAKES, *Strong cosserat elasticity in a transversely isotropic polymer lattice*, Physical Review Letters, (2018).
- [50] O. SANDER, *Geodesic finite elements for Cosserat rods*, International journal for numerical methods in engineering, 82 (2010), pp. 1645–1670.
- [51] J. SCHÖBERL, *NETGEN an advancing front 2D/3D-mesh generator based on abstract rules*, Computing and Visualization in Science, 1 (1997), pp. 41–52.
- [52] ———, *C++ 11 implementation of finite elements in NGSolve*, Institute for Analysis and Scientific Computing, Vienna University of Technology, (2014).
- [53] Y. SHANG, C.-F. LI, AND K.-Y. JIA, *8-node hexahedral unsymmetric element with rotation degrees of freedom for modified couple stress elasticity*, International Journal for Numerical Methods in Engineering, 121 (2020), pp. 2683–2700.
- [54] Y. SHANG, Z.-H. QIAN, S. CEN, AND C.-F. LI, *A simple unsymmetric 4-node 12-DOF membrane element for the modified couple stress theory*, International Journal for Numerical Methods in Engineering, 119 (2019), pp. 807–825.
- [55] A. SINWEL, *A New Family of Mixed Finite Elements for Elasticity*, PhD thesis, Johannes Kepler Universität Linz, Linz, 2009.
- [56] R. STENBERG, *Postprocessing schemes for some mixed finite elements*, ESAIM: Mathematical Modelling and Numerical Analysis, 25 (1991), pp. 151–167.
- [57] H.-P. WU, Y. SHANG, S. CEN, AND C.-F. LI, *Penalty C0 8-node quadrilateral and 20-node hexahedral elements for consistent couple stress elasticity based on the unsymmetric finite element method*, Engineering Analysis with Boundary Elements, 147 (2023), pp. 302–319.
- [58] Q. XIE, Y. HU, Y. ZHOU, AND W. HAN, *Improving the bending response of four-node quadrilateral and eight-node hexahedral elements for Cosserat elasticity problems*, Engineering Computations, 36 (2019), pp. 1950–1976.

SUNY POLYTECHNIC INSTITUTE, UTICA NY 13502, USA

Email address: `dziubea@sunypoly.edu`

THE UNIVERSITY OF EDINBURGH, JAMES CLERK MAXWELL BUILDING, PETER GUTHRIE TAIT RD, EDINBURGH
EH9 3FD, UK

Email address: `kaibo.hu@ed.ac.uk`

TECHNISCHE UNIVERSITÄT BERLIN, BERLIN, DE

Email address: `karow@math.tu-berlin.de`

PORTLAND STATE UNIVERSITY, PO BOX 751, PORTLAND OR 97201, USA

Email address: `mneunteu@pdx.edu`